On the whistling of corrugated pipes: effect of pipe length and flow profile

G. NAKIBOĞLU[1]†, S. P. C. BELFROID[2], J. GOLLIARD[2] AND A. HIRSCHBERG[1]

[1]Department of Applied Physics, Eindhoven University of Technology, PO Box 513, 5600 MB Eindhoven, The Netherlands

[2]TNO Science and Industry, 2600 AD Delft, The Netherlands

Whistling behaviour of two geometrically periodic systems, namely corrugated pipes and multiple side branch systems, is investigated both experimentally and numerically. Tests are performed on corrugated pipes with various lengths and cavity geometries. Experiments show that the peak-whistling Strouhal number, where the maximum amplitude in pressure fluctuations is registered, is independent of the pipe length. Experimentally, a decrease of the peak-whistling Strouhal number by a factor of two is observed with increasing confinement ratio, i.e. the ratio of pipe diameter to cavity width. A numerical methodology that combines incompressible flow simulations with vortex sound theory is proposed to estimate the acoustic source power in periodic systems. The methodology successfully predicts the Strouhal number ranges of acoustic energy production/absorption and the nonlinear saturation mechanism responsible for the stabilization of the limit cycle oscillation. The methodology predicts peak-whistling Strouhal numbers in agreement with experiments and explains the dependence of the peak-whistling Strouhal number on the confinement ratio. Combined with an energy balance, the proposed methodology is used to estimate the acoustic fluctuation amplitudes.

1. Introduction

In thin walled pipes, corrugations make the structure locally stronger while keeping its global flexibility. This unique characteristic makes corrugated pipes convenient for various industrial utilizations. However, at critical conditions, the flow through these pipes causes self-sustained oscillations that lead to high-amplitude sound generation, called whistling. These noise problems are encountered in applications such as domestic appliances, ventilation systems and heat exchangers (Petrie & Huntley 1980; Elliott 2005). For applications at elevated operating pressures such as offshore natural gas production systems, self-sustained oscillations also lead to dangerous structural vibrations (Belfroid, Shatto & Peters 2007; Goyder 2009).

In corrugated pipes, sound generation is due to an oscillation driven by a flow-acoustic interaction as pointed out by Burstyn (1922) and Cermak (1922). Flow separation occurring at the upstream edge of each cavity generates a shear layer

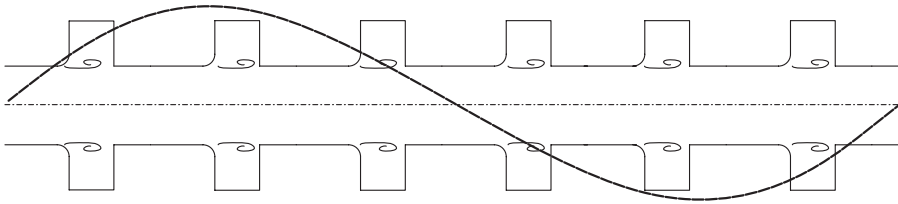† Email address for correspondence: g.nakiboglu@tue.nl

FIGURE 1. Schematic representation of a corrugated pipe, shear layers at the cavity openings and acoustic field for the second longitudinal standing wave.

(see figure 1), which is a source of unsteadiness. This unsteady flow induces an unsteady force on the walls bounding the flow. The reaction force of the walls to this hydrodynamic force is the source of sound (Gutin 1948; Curle 1955).

Note that the flexibility of the tube is not a necessary facet for the sound generation in corrugated tubes, as shown by Nakamura & Fukamachi (1991). However, a mechanical vibration induced by the unsteady forcing on the walls can have a significant effect. For water flow, Ziada & Bühlmann (1991) observed a strong coupling of whistling with pipe wall vibrations.

A more frequently observed coupling of shear layers occurs with longitudinal acoustic standing waves in the pipe, see figure 1 (Petrie & Huntley 1980; Nakamura & Fukamachi 1991; Kristiansen & Wiik 2007; Kop'ev, Mironov & Solntseva 2008; Nakiboğlu *et al.* 2010). The resulting high-amplitude oscillations control the vortex shedding (Rockwell 1983; Bruggeman *et al.* 1991). These kinds of flow pulsations are called self-sustained oscillations, which can be explained through a feedback loop composed of a hydrodynamic and an acoustic subsystem (Nakamura & Fukamachi 1991; Tonon *et al.* 2010). The shear-layer instability, which is the hydrodynamic subsystem, acts as an amplifier and supplies acoustic energy to the system. Longitudinal standing waves, which are the acoustic subsystem, act as a band-pass filter and maintain the synchronization in this feedback mechanism. This band-pass filter is the reason for stepwise increase of the whistling frequency at certain flow velocities, which has been pointed out in numerous experimental studies (Binnie 1961; Crawford 1974; Silverman & Cushman 1989; Cadwell 1994; Elliott 2005; Kristiansen & Wiik 2007; Kop'ev *et al.* 2008). Each step corresponds to the resonance frequency of an acoustic mode. Another widely observed characteristic is that for each corrugated pipe, the whistling frequencies are close to a single non-dimensional frequency, called Strouhal number, which is discussed in detail in §2.3.

Depending on the application, geometric parameters of corrugated pipes may vary in a fairly large range and it is known that these parameters have a significant effect on the whistling phenomena (Petrie & Huntley 1980; Nakiboğlu *et al.* 2010). Thus, in the course of designing silent corrugated pipes, it is an asset for industry to be able to estimate quantitatively the effect of modifications in geometric parameters on the whistling. In figure 2, relevant geometric parameters are shown for two generic corrugated pipe cross-sections. Corrugations form a periodic variation of the inner diameter of the pipe. The wavelength of a corrugation is called pitch (Pt). Depending on structural requirements and manufacturing technique, the cavity geometries of corrugated pipes can also vary in complexity. In the simplest case (see figure 2a), each corrugation is a slit-shaped cavity with a width (W) and a depth (H). The radii of the edges are denoted by r_{up} and r_{down} for upstream and downstream edges, respectively. The plateau (l) is defined as the length of the constant inner diameter (D_p) part between two cavities. Another commonly used corrugated pipe with a simple cavity
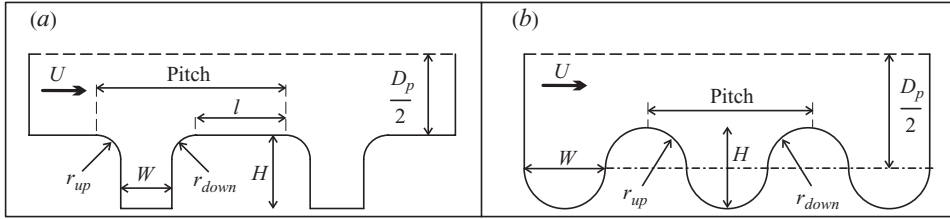
FIGURE 2. Typical cross-sections of corrugated pipes with geometric parameters:
(*a*) Nakiboğlu *et al.* (2010) and Tonon *et al.* (2010); (*b*) Binnie (1961) and Elliott (2005).

geometry is shown in figure 2(*b*) (Binnie 1961). There is no plateau between cavities and since the cavity width changes continuously with the cavity depth, width (W) is defined at the mid-depth of the cavity (Elliott 2005).

It should be noted that axisymmetry of the cavities is not a necessary feature of the whistling phenomenon observed in corrugated pipes. Experiments performed with a multiple side branch system, which is a non-axisymmetric system with a periodically changing cross-section area along the pipe length, exhibit a whistling behaviour similar to that of corrugated pipes (Nakiboğlu *et al.* 2009, 2010; Tonon *et al.* 2010). Another important result obtained by Nakiboğlu *et al.* (2010) is that the whistling amplitude is independent of the depth (H) for $1.2 \geqslant H/W \geqslant 0.5$. For shallow cavities ($H/W \leqslant 0.5$), on the other hand, the whistling amplitude depends on the depth. In this study, only the $H/W \geqslant 0.5$ range is addressed.

Experiments on the localization of the region of sound production in periodic systems have shown that the contribution of each cavity or side branch to the sound production is not the same (Golliard, Tonon & Belfroid 2010; Nakiboğlu *et al.* 2010; Tonon *et al.* 2010). Their individual contributions depend on their positions with respect to the shape of the coupling acoustic standing wave. It was demonstrated that the sound production is dominant within the regions of high grazing acoustic velocities, which are located around the acoustic pressure nodes of the coupling standing wave along the main pipe.

Another outcome of earlier studies (Elliott 2005; Nakiboğlu *et al.* 2010; Tonon *et al.* 2010) is that acoustic waves in periodic systems propagate at an effective speed of sound (c_{eff}), which is lower than the speed of sound (c_0). Assuming that the acoustic compliance is determined by the pitch volume, $\pi D_p[(Pt\, D_p/4) + HW]$, and the inertia is determined by the mass in the main pipe, $\rho Pt\, \pi D_p^2/4$, the effective speed of sound for low frequency, $fPt/c_0 \ll 1$, acoustic waves along the pipe can be estimated as follows:

$$c_{eff} = c_0/\sqrt{1 + V_c/(S_p Pt)}, \qquad (1.1)$$

where $S_p = \pi D_p^2/4$ is the cross-sectional area of the tube and $V_c = \pi D_p HW$ is the cavity volume.

In this paper both experimental and numerical investigations of whistling in periodic systems are reported. The first part of the paper is dedicated to the experimental results. In §2.1, experimental set-ups are presented, followed by §2.2, where the periodic systems that have been tested are introduced with the respective geometric details. Before presenting the experimental results, §2.3 is devoted to a detailed discussion of Strouhal numbers in periodic systems. In §§2.4–2.6, the effects of system length, helical configuration and confinement ratio on whistling are addressed, respectively. In the second part of the paper, a numerical methodology is proposed and appraised for the investigation of the aeroacoustic response of whistling periodic
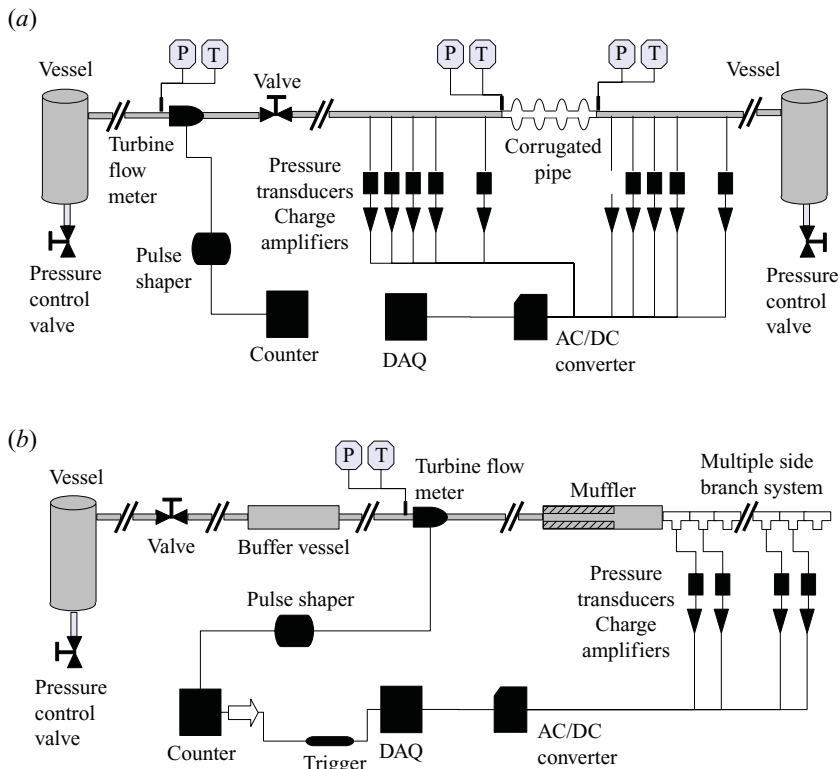
FIGURE 3. (Colour online) Experimental set-ups for (*a*) the corrugated pipe and (*b*) the multiple side branch system.

systems (§§ 3.1–3.3). Then, in § 3.4, using the proposed methodology, the reason for the broad range of Strouhal numbers observed in periodic systems is clarified. In §§ 3.5 and 3.6, the capability of the method in predicting pressure fluctuation amplitudes in whistling periodic systems is explored. In § 3.7, the limitations of the proposed approach and the possible improvements are reviewed. In the last section, the conclusions are stated.

2. Experiments

2.1. *Experimental set-ups*

Different experimental set-ups were employed to test corrugated pipes and multiple side branch systems. Pressure fluctuations could easily be measured in the multiple side branch system by means of flush-mounted microphones placed at the end of side branches. For corrugated pipes, however, positioning microphones directly on the walls is very difficult. Consequently, for a reliable installation of flush-mounted microphones, straight pipe segments were used both upstream and downstream of the corrugated pipes under investigation. These two experimental set-ups are briefly described below (Nakiboğlu *et al.* 2010; Tonon *et al.* 2010).

The schema of the experimental set-up employed in corrugated pipe experiments is shown in figure 3(*a*). From upstream to downstream, the set-up is composed of a pressure vessel, a turbine flow meter, a flow control valve, a measurement section, a corrugated pipe segment, a second measurement section and a pressure vessel. Using

the downstream pressure control valve, the system can be pressurized up to 12 bar, which allows the testing of the Reynolds number dependence of the system (Belfroid *et al.* 2007). The constant diameter, $D = 50.8$ mm (2 in.), upstream and downstream measurement sections are each 1.6 m long and equipped with five flush-mounted microphones. By means of a multi-microphone method (Åbom & Bodén 1988; Peters *et al.* 1993) travelling acoustic plane waves were reconstructed. Corrugated pipe segments with various cavity geometries and lengths were tested between the two measurement sections. To calculate the flow velocity in the test section from the volume flow measurement, pressure (p) and temperature (T) measurements were recorded at three different locations, the first one close to the turbine flow meter (p_{meter}, T_{meter}), the second one upstream (p_{up}, T_{up}) and the third one downstream (p_{down}, T_{down}) of the test section. By doing so the pressure drop and the change in temperature through the pipe are taken into account. This becomes essential for corrugated pipes longer than 10 m. The flow velocities at the upstream and downstream terminations of the test section are determined as follows:

$$U_{up} = \frac{Q_{meter}}{S_p} \frac{T_{up}}{T_{meter}} \frac{p_{meter}}{p_{up}}, \quad U_{down} = \frac{Q_{meter}}{S_p} \frac{T_{down}}{T_{meter}} \frac{p_{meter}}{p_{down}}, \quad (2.1)$$

where Q_{meter} is the volumetric flow rate measured by the turbine flow meter and S_p is the minimum cross-sectional area of the corrugated pipe. The flow velocity in the test section is taken as the arithmetic average of the upstream and downstream flow velocities, $U = (U_{up} + U_{down})/2$.

The set-up used for the multiple side branch system experiments is shown in figure 3(*b*). The upstream termination of the multiple side branch system is connected to the high-pressure air supply system, which is composed of, from upstream to downstream, a compressor, a vessel, a control valve, a buffer vessel, a turbine flow meter and an expansion chamber muffler. The downstream termination is open to the laboratory, a large room of 15 m × 4 m × 4 m. Even the longest multiple side branch system which was employed in the experiments (≈ 2 m), is short enough to neglect changes in flow velocity through the system due to pressure drop. Thus, it was not necessary to make pressure and temperature measurements at multiple locations as in corrugated pipe experiments.

In both set-ups, the microphones (PCB 116A) are connected to charge amplifiers (Kistler 5011). These amplifiers are connected to a PC through an AC/DC converter acquisition board (National Instruments NI SCXI-1000). A turbine flow meter (Instromet SM-RI-X-KG250) is used to measure the volumetric flow rate. The turbine flow meter is connected to a pulse shaper and a counter. In the set-up for the multiple side branch system, the turbine flow meter and the piezo-electric pressure transducers are synchronized by means of a trigger. The simultaneous measurement of flow velocity and pressure allows a waterfall representation of the data, in which the frequency spectra of the whistling at different flow velocities are presented in a single graph. This interpretation can capture consecutive modes that appear simultaneously with the dominant hydrodynamic mode, as observed in the literature for single axisymmetric cavities (Rockwell *et al.* 2003; Oshkai, Rockwell & Pollack 2005). However, during the experimental campaign, secondary modes were not observed.

2.2. *Corrugated pipes and multiple side branch system*

Throughout the experimental campaign both commercially available corrugated pipes and corrugated pipes manufactured from polyvinyl chloride (PVC) tubes were used,

Sample	W (mm)	H (mm)	r_{up} (mm)	r_{down} (mm)	l (mm)	Sample	W (mm)	H (mm)	r_{up} (mm)	r_{down} (mm)	l (mm)
Geo 1	8.0	4.0	2.0	2.0	0	Geo 7	4.0	4.0	0.0	0.0	8.0
Geo 2	4.0	4.0	2.0	2.0	4.0	Geo 8A	2.0	2.0	2.0	0.5	5.5
Geo 3A	4.0	4.0	3.0	1.0	4.0	Geo 8B	2.0	2.0	0.5	2.0	5.5
Geo 3B	4.0	4.0	1.0	3.0	4.0	Geo 9	2.0	4.0	2.0	2.0	4.0
Geo 4	4.0	4.0	2.0	2.0	0	Geo 10	2.0	2.0	2.0	2.0	4.0
Geo 5	4.0	4.0	2.0	2.0	8.0	Com 1	0.6	1.7	1.1	1.4	5.2
Geo 6A	4.0	4.0	4.0	0.0	4.0	Com 2	0.6	1.8	1.6	1.3	4.7
Geo 6B	4.0	4.0	0.0	4.0	4.0	Com 3	7.0	5.0	1.5	1.5	0

TABLE 1. Geometric parameters of tested corrugated pipes (Geo, PVC corrugated pipes; Com, commercial corrugated pipes).
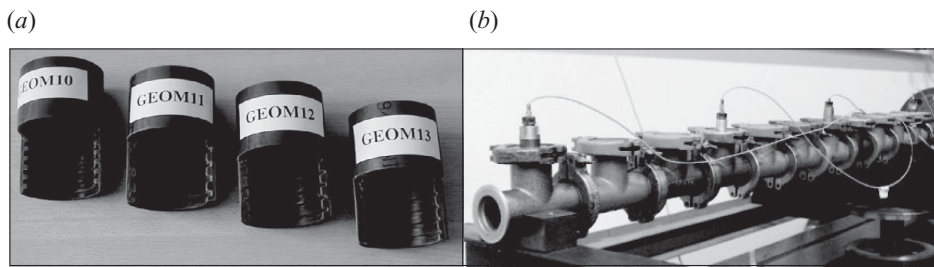
(*a*) (*b*)

FIGURE 4. Samples of corrugated pipes manufactured from PVC (*a*) and multiple side branch system (*b*).
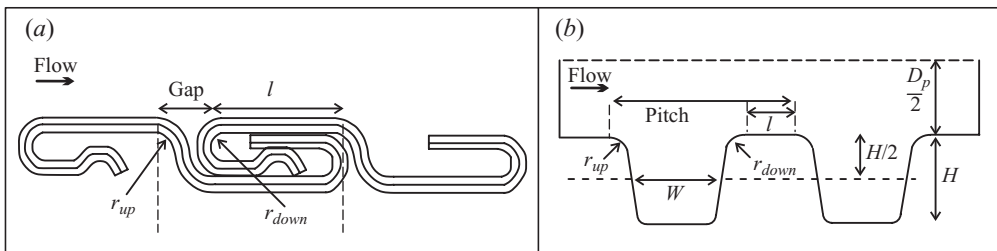

FIGURE 5. Schematic drawing of commercially available corrugated pipes: (*a*) Com 1 and Com 2 and (*b*) Com 3 in table 1.

see figure 4(*a*). The geometric parameters of the tested pipes are specified in table 1. The pipes with asymmetric cavity geometries are tested in both flow directions and corresponding samples denoted configurations A and B of the same pipe. The cavity geometries of the commercial corrugated pipes (Com 1 and Com 2) are quite different from those of PVC pipes (Geo), see figure 5(*a*). The technical specifications of the pipes obtained from the manufacturers are also presented in table 1. Com 3 is another commercially available corrugated pipe. It has a relatively simple cavity shape (see figure 5*b*) similar to that of the PVC corrugated pipes. For all geometries, the inner diameter of the pipe (D_p) is 50 ± 1 mm.

The multiple side branch system is made of a series of identical T-joints connected to each other, forming a row of equally spaced side branches along a main pipe, see figure 4(*b*). The T-joint elements are standard vacuum appliances (ISO-KF) cast in aluminium. The main pipe of the T-joint has a diameter (D_p) of 33 mm, which is equal to the diameter of the side branch (D_{sb}). The length of the main pipe of each

T-joint is 100 mm and the side branch, located half way along this segment, has a length (L_{sb}) of 33 mm. The upstream edge of the side branch, which is connected to the main pipe, has a radius of curvature of $r_{up} = 3$ mm, which is approximately one tenth of the side branch diameter ($r_{up}/D_{sb} \approx 0.1$). T-joints are connected to each other using standard ISO-KF clamps which incorporate O-rings for sealing.

2.3. *Definition of Strouhal number for whistling periodic systems*

The Strouhal number is a commonly used dimensionless parameter for oscillating flows, as in the case of whistling. The Strouhal number is defined as

$$Sr = \frac{fL}{U}, \tag{2.2}$$

where f is the frequency of the oscillation, L is the characteristic length and U is the average flow speed inside the corrugated pipe. Average flow speed U is defined in terms of the volumetric flow rate (Q) and the inner diameter of the pipe as

$$U = 4Q/(\pi D_p^2) \tag{2.3}$$

The wavelength of the corrugations, the pitch, has been a commonly used characteristic length (Binnie 1961; Crawford 1974; Nakamura & Fukamachi 1991; Serafin & Kojs 2005; Popescu & Johansen 2008). However, testing pipes with more marked differences between cavity width and pitch showed that the peak-whistling Strouhal number depends on the cavity width rather than on the pitch (Elliott 2005; Belfroid *et al.* 2007; Kristiansen & Wiik 2007; Nakiboğlu *et al.* 2010; Tonon *et al.* 2010). It was also concluded that the characteristic length used in the Strouhal number definition should include the upstream edge radius (r_{up}) because of the increase in the distance travelled by the vorticity perturbation due to rounding off the upstream edge. The downstream edge radius is less critical because vortical perturbations at the upstream edge of the cavity diffuse as they are swept along the cavity mouth. When they reach the downstream edge, they are less localized than when they are close to the upstream edge. As a consequence, the radius of the downstream edge (r_{down}) does not affect the travel time of the perturbations (Bruggeman *et al.* 1991; Belfroid *et al.* 2007; Nakiboğlu *et al.* 2009) as significantly as that of the upstream edges. Following this, the sum of the cavity width and the upstream edge radius, $W + r_{up}$, appears to be the most suitable characteristic length, which is used in the remainder of this paper.

It is important to realize that since the peak-whistling Strouhal number is independent of the pitch length, the distance between the cavities, plateau length (l), is not important for the sound production (Nakiboğlu *et al.* 2010). This implies that sound production is a local effect which can be, in a first-order approximation, studied for a single cavity. In the present analysis the possible hydrodynamic interaction between successive cavities is neglected.

Another point that should be highlighted is that within a specific resonant mode with increasing flow velocity, the whistling frequency shows a slight increase (Sarohia 1977; Bruggeman *et al.* 1991; Ziada, Ng & Blake 2003). Thus, within the same resonant mode, as the flow velocity in the main pipe increases, the Strouhal number decreases. As a result, for each resonant mode there is a range of Strouhal numbers in which the whistling phenomenon is observed. The highest Strouhal number for a resonant mode is called the critical Strouhal number (Sr_{cr}), because it indicates the onset of oscillations for that particular acoustic mode. After the onset of resonance, within the same resonant mode, increasing the flow velocity increases the amplitude

of pressure oscillations till it reaches a peak value. Further increase of the flow velocity decreases the amplitude of pressure fluctuations. The Strouhal number which corresponds to the maximum pressure fluctuation amplitude for a given acoustical mode is called peak-whistling Strouhal number ($Sr_{p\text{-}w}$). The former is crucial in developing design charts to avoid acoustic resonances by predicting the critical flow velocities (Ziada & Shine 1999). The latter is also important in the estimation of the maximum amplitudes that the system will experience (Tonon *et al.* 2010). The peak-whistling Strouhal number of a corrugated pipe is determined through a linear least-squares fit of consecutive excited acoustic modes (Nakiboğlu *et al.* 2010).

The definition of the Strouhal number in multiple side branch systems is similar to that of corrugated pipes. Instead of using the sum of cavity width and upstream edge radius ($W + r_{up}$) as characteristic length, the sum of the effective cavity width and upstream edge radius ($W_{eff} + r_{up}$) is used. This distinction in the characteristic length is due to a geometric difference between corrugated pipes and multiple side branch systems. The cross-section of a corrugation cavity is a slit whereas the side branches have circular cross-sections, see figure 4(*b*). Thus, the side branch diameters are converted to an effective cavity width ($W_{eff} = \pi D_{sb}/4$) as proposed by Bruggeman *et al.* (1991), which is the average width of the side branch cross-section.

There is also a difference in the determination of peak-whistling Strouhal number between corrugated pipes and multiple side branch systems. The corrugated pipes (Geo, table 1) used in this study have typically 2×10^2 corrugations, whereas the multiple side branch systems used in the experiments are composed of 14–19 T-joints. Whistling frequencies that are observed with corrugated pipes are rather high compared with those in the multiple side branch system. Thus, the typical number of corrugations per wavelength in corrugated pipes at high frequencies ($fL/c_{eff} = O(10)$) is close to that of the multiple side branch systems at low frequencies ($fL/c_{eff} = O(1)$) (Nakiboğlu *et al.* 2010; Tonon *et al.* 2010). Correspondingly, in the multiple side branch systems, attention is only paid to the lowest acoustical modes.

2.4. *Effect of pipe length on the whistling behaviour of periodic systems*

Though there is an extensive literature on corrugated pipes, in many instances it is limited to short pipe segments (Binnie 1960, 1961; Crawford 1974; Cadwell 1994; Elliott 2005; Popescu & Johansen 2008). Ziada & Bühlmann (1991) investigated long corrugated pipes with water flow. They observed a strong coupling between whistling and pipe wall vibrations. For gas flows such an effect of wall vibration has not been observed. Here the effect of pipe length (L_p) on the whistling phenomenon is addressed, which has been a subject of limited consideration. Experiments have been performed with commercially available corrugated pipes (Com 3 in table 1) with lengths of 20, 40, 60, 100 and 200 pipe diameters. The whistling frequencies are plotted as a function of Mach number (M) in figure 6(*a*). Linear least-square fits used for the determination of peak-whistling Strouhal numbers for $L_p/D_p = 20$ and $L_p/D_p = 200$ are also shown. It is seen that the peak-whistling Strouhal number is independent of the length of the pipe segment, with the value $Sr_{p\text{-}w} = 0.49 \pm 0.04$. In figure 6(*b*), the dimensionless pressure fluctuation amplitude as a function of Mach number is given for the same five corrugated pipe segments. The dimensionless amplitude, $|p'_{max}|/\rho c_0 U = |u'_{max}|/U$, is defined as the amplitude of the standing pressure wave at a pressure anti-node inside the main pipe $|p'_{max}|$, divided by the air density ρ, the speed of sound c_0 and the main flow velocity U; it is equal to the amplitude of the acoustic velocity at a pressure node inside the main pipe $|u'_{max}|$ divided by the main flow velocity U. An increase in pressure fluctuation amplitude is observed with
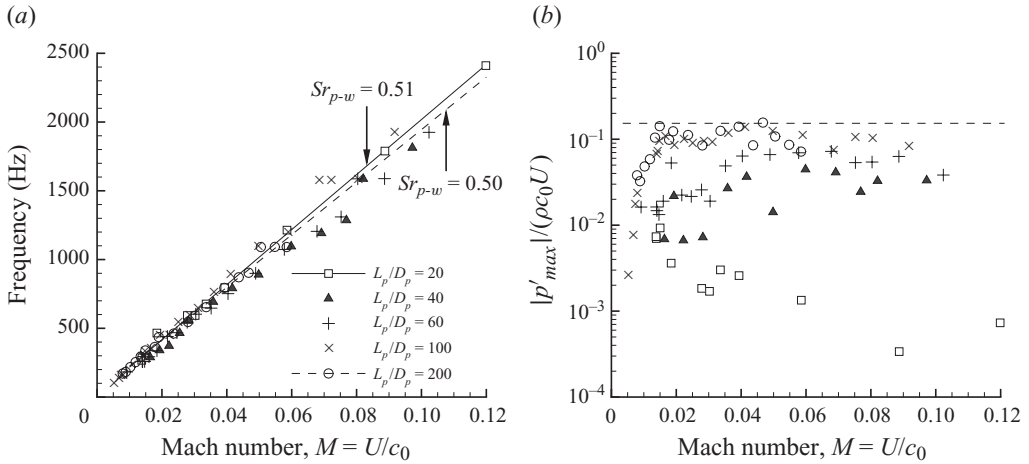
FIGURE 6. Experiments performed with a commercial corrugated pipe (Com 3 in table 1) with five different pipe lengths between $L_p/D_p = 20$ and $L_p/D_p = 200$. (*a*) Whistling frequency plotted against Mach number and (*b*) dimensionless pressure fluctuation amplitude $|p'_{max}|/\rho c_0 U$ plotted against Mach number.
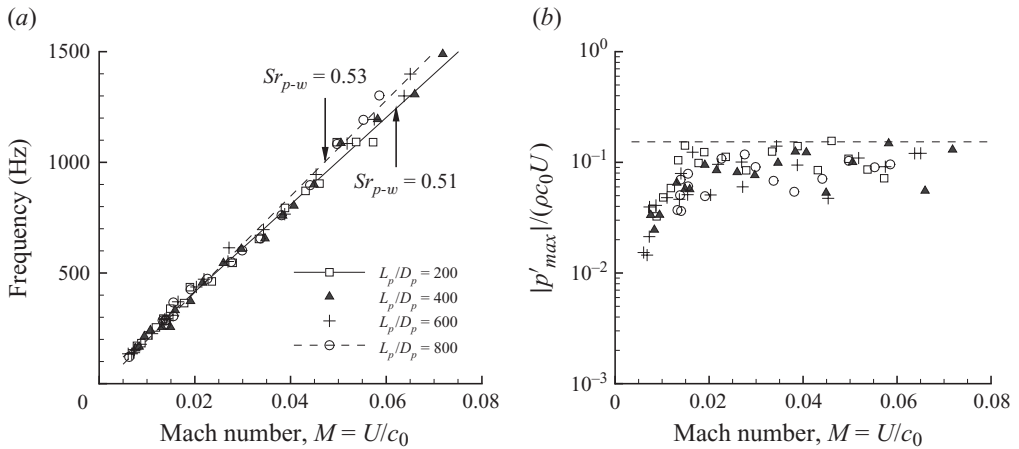

FIGURE 7. Experiments performed with a commercial corrugated pipe (Com 3 in table 1) with four different pipe lengths between $L_p/D_p = 200$ and $L_p/D_p = 800$. (*a*) Whistling frequency plotted against Mach number and (*b*) dimensionless pressure fluctuation amplitude $|p'_{max}|/\rho c_0 U$ plotted against Mach number.

increasing corrugated pipe length until L_p/D_p of 100. Further increase of the pipe length to $L_p/D_p = 200$ does not change the amplitude. A saturation of dimensionless pressure fluctuation amplitude is observed at $|p'_{max}|/\rho c_0 U \approx 0.1$.

Experiments were also performed with corrugated pipe segments (L_p/D_p) of 400, 600 and 800, as shown in figure 7. It is also clear that for these long corrugated pipe segments (up to 4000 pitch lengths), the peak-whistling Strouhal number does not depend significantly on the length of the pipe segment. It is evident that the saturation level of pressure fluctuation amplitude $|p'_{max}|/\rho c_0 U \approx 0.1$ is also independent of the pipe length.
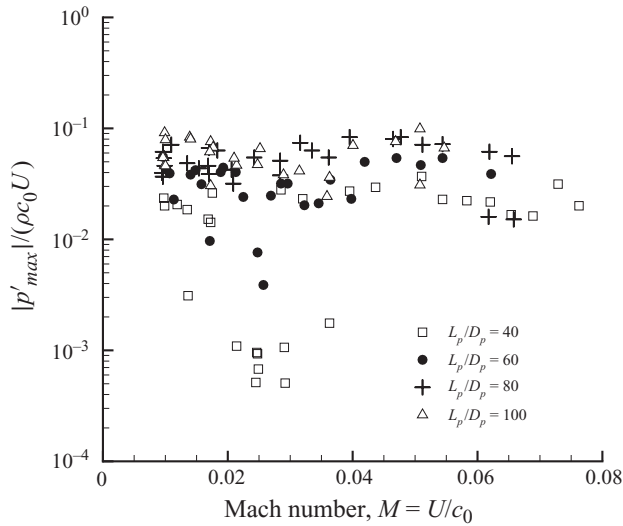
FIGURE 8. Dimensionless pressure fluctuation amplitude $|p'_{max}|/\rho c_0 U$ plotted against Mach number for a PVC corrugated pipe (Geo 4 in table 1) with four different pipe lengths between $L_p/D_p = 40$ and $L_p/D_p = 100$.

The saturation in pressure fluctuation amplitude is also observed with corrugated pipes manufactured from PVC, with simple cavity geometries. As demonstrated in figure 8 for Geo 4 (table 1), pressure fluctuations have already reached a saturation amplitude of $|p'_{max}|/\rho c_0 U \approx 0.1$ by L_p/D_p of 60. Testing longer pipes $L_p/D_p = 80$ and $L_p/D_p = 100$ does not further increase the fluctuation amplitude. This saturation amplitude in corrugated pipes is considerably lower than those observed for deep closed side branches in the crossflow direction $|u'_{max}|/U \approx O(1)$ (Kriesels *et al.* 1995; Ziada & Shine 1999; Dequand, Hulshoff & Hirschberg 2003a) and along the main flow direction $|u'_{max}|/U \approx 0.6$ (Bruggeman *et al.* 1991) as well as Helmholtz resonators $|u'_{max}|/U \approx 0.6$ (Dequand *et al.* 2003b).

Multiple side branch systems with different numbers of T-joints were constructed for the study, from 14 for the shortest system to 19 for the longest. In figure 9, measured dimensionless pressure fluctuation amplitudes for the third acoustic mode are plotted as a function of Strouhal number. Similar to corrugated pipes, the peak-whistling Strouhal number remains unaltered with changing system length and is 0.62 ± 0.01. Also, a saturation in the pressure fluctuation at $|p'_{max}|/\rho c_0 U \approx 0.035$ is reached for 19 side branches. This is close to the level found for corrugated pipes of equal length ($L_p/D_p = 40$).

2.5. *Effect of helical corrugations*

Experiments have been performed to investigate the whistling behaviour of helical (spiral wound) corrugated pipes. A corrugated pipe is manufactured with the same cavity geometry as Geo 4 (table 1) but with a helical configuration, instead of a periodic arrangement of cavities as shown in figure 2. The pitch, which is the width of one complete helix, is also the same as the pitch length of Geo 4.

Introducing helical corrugations in this case has no significant effect on the whistling behaviour. Observed fluctuation amplitudes and respective saturation level remain the same. A slightly lower peak-whistling Strouhal number $St_{p\text{-}w} = 0.34$ is recorded with the helical configuration compared with the periodic configuration $St_{p\text{-}w} = 0.38$.
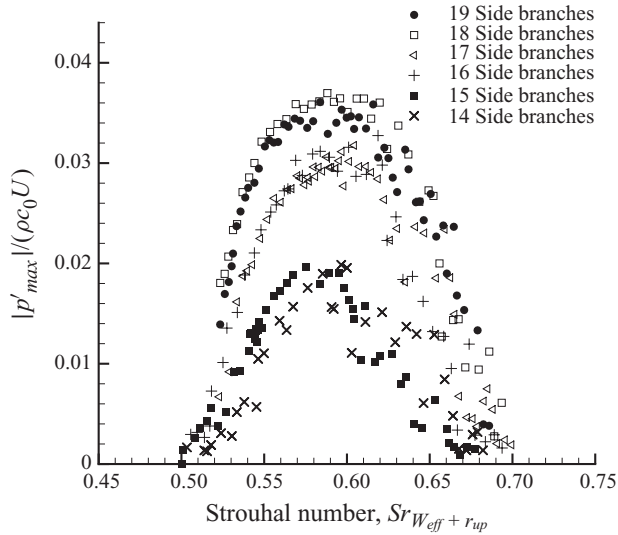
FIGURE 9. Dimensionless pressure fluctuation amplitude $|p'_{max}|/\rho c_0 U$ plotted against the Strouhal number $Sr_{W_{eff}+r_{up}}$ for the third acoustic mode for multiple side branch systems that are composed of different numbers of T-joints.

Experiments on helical corrugated pipes reported by Kop'ev et al. (2008) also indicate a behaviour analogous to that of non-helical (periodic) corrugated pipes.

2.6. Effect of confinement ratio on the Strouhal number in periodic systems

In periodic systems, a broad range of peak-whistling Strouhal numbers has been observed. For corrugated pipes, a range between $0.3 \leqslant Sr_{p-w} \leqslant 0.5$ has been found (Binnie 1961; Petrie & Huntley 1980; Nakamura & Fukamachi 1991; Nakiboğlu et al. 2010). For multiple side branch systems, a relatively high peak-whistling Strouhal number $Sr_{p-w} = 0.6$ has been recorded (Tonon et al. 2010). Binnie (1961) explained this wide range of Strouhal numbers as an outcome of the confinement ratio, which is defined as the ratio of pipe diameter to cavity width (D_p/W). He used a single corrugated pipe but by using rods of different diameters (D_r) placed coaxially inside the pipe, he was able to vary the confinement ratio. In the presence of a rod, the confinement ratio is defined as (($D_p - D_r$)/W). As mentioned in § 2.3, in the case of rounded cavity edges, it is essential to include the value of r_{up} in the characteristic length. Thus, here the confinement ratio is modified as $(D_p - D_r)/(W + r_{up})$. Unfortunately, Binnie (1961) did not provide any explicit information on the edge geometry of the cavities. However, by comparing commercial corrugated pipes (see figure 2b) similar to those mentioned in his paper, the edge radius is estimated as 25 % of the cavity width. Then, it is concluded that Binnie (1961) observed a shift in the peak-whistling Strouhal number from 0.53 to 0.34 with an increasing confinement ratio $(D_p - D_r)/(W + r_{up})$ from 2.8 to 9.6. In figure 10, peak-whistling Strouhal number data are presented as a function of confinement ratio for the corrugated pipes (table 1) and the multiple side branch system, together with the measurements of Binnie (1961) and Elliott (2005). A decrease in the peak-whistling Strouhal number with increasing confinement ratio is found. Though these experiments clearly demonstrate the shift of the peak-whistling Strouhal number due to confinement, the reason for the shift remains elusive. In experiments with a tandem side branch configuration, Ziada & Shine (1999) observed a similar shift in
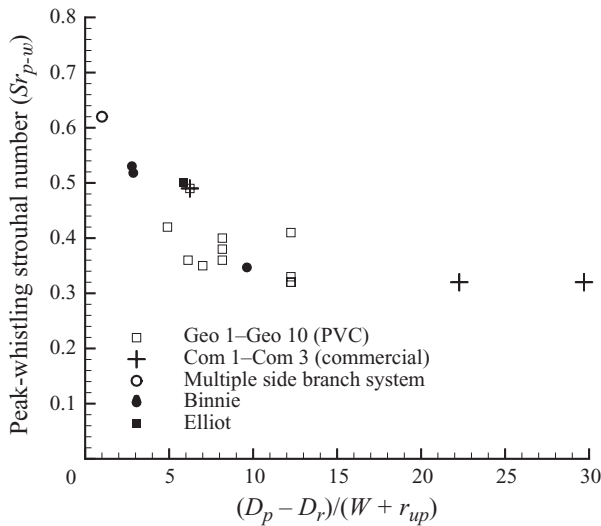
FIGURE 10. Peak-whistling Strouhal number plotted against confinement ratio, $(D_p - D_r)/(W + r_{up})$, for various periodic systems (Binnie 1961; Elliott 2005)

the peak-whistling Strouhal number with increasing ratio of the main pipe diameter to side branch diameter (D_p/D_{sb}). Ziada & Shine (1999) suggested that the shift in the peak-whistling Strouhal number was due to a decrease in the ratio of cavity width to gradient length of the velocity profile of the approach flow. This will be addressed in detail in §3.4.

3. Numerical methodology

In this section, a new numerical technique is introduced to investigate the whistling in periodic systems. As mentioned in §1, the self-oscillations observed in periodic systems are due to a feedback loop, in which the shear-layer instability and the longitudinal standing wave act as an amplifier and a filter, respectively. The proposed technique is developed to study only the amplifier of this feedback loop and the velocity fluctuations controlling the shear-layer oscillations are imposed as inlet boundary conditions. As explained in §2.3, by neglecting a possible hydrodynamic interaction between successive cavities, sound generation in periodic systems can be studied, in a first-order approximation, on a single cavity. The method combines incompressible flow simulations with vortex sound theory to estimate the strength of an acoustic source due to the interaction of a single cavity in a pipe flow at high Reynolds number with a low frequency acoustic field. In the following two sections, these two parts of the approach are explained. Then, the proposed numerical methodology is used to explain some of the phenomena observed in whistling periodic systems such as the nonlinear saturation of the amplitude and the effect of confinement ratio on the peak-whistling Strouhal number.

3.1. *Incompressible simulations*

In corrugated pipes, the cavity width of the corrugations and respectively in multiple side branch systems the diameter of the side branches are usually small compared with the wavelength (λ) of the standing waves $(Pt/\lambda < 10^{-1})$. The flow in such a cavity/side branch can be assumed to be locally incompressible. Accordingly, unsteady
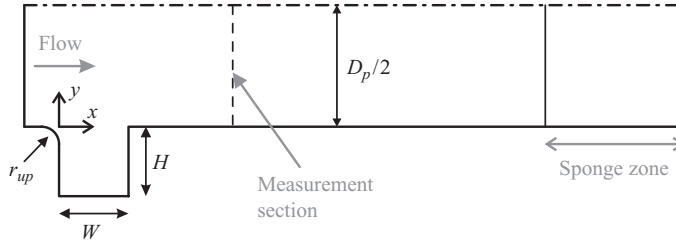
FIGURE 11. The domain and the relevant geometric parameters, axis of symmetry (cylindrically symmetric flow) or upper wall (plane flow) (— - —).

incompressible flow simulations are performed (Martínez-Lera *et al.* 2009) for a single cavity in a confined flow. All the simulations are performed in two-dimensional (2D) domains. The domain and the relevant geometric parameters are shown in figure 11. In some simulations, cylindrical symmetric domains are used to mimic a circumferential cavity as found in corrugated pipes. In those simulations, the upper wall of the confining pipe is replaced by an axis of symmetry. The inner diameter of the pipe is denoted by D_p, the depth of the cavity by H, the width of the cavity by W and the radius of curvature of the upstream cavity edge by r_{up}. The inlet is located at $0.5W$ upstream of the cavity; such a short inlet pipe section is chosen to make sure that the imposed inlet velocity profiles do not evolve significantly before reaching the cavity. The outlet is placed at a reasonably far location, $9W$ downstream, from the cavity. In all the simulations, the cavity depth is taken equal to the cavity width. A previous experimental study (Nakiboğlu *et al.* 2010) showed that $H/W = 1$ is in the range $(0.5 \leqslant H/W \leqslant 1.2)$ where a saturation behaviour is observed in the amplitude of pressure fluctuations. In this range, variations in the H/W ratio neither influence the amplitude nor the peak-whistling Strouhal number. Unless mentioned otherwise, in all the simulations the upstream cavity edge radius is taken as $r_{up} = 0.25W$, which is a typical value for corrugated pipes, see figure 2(*b*).

A finite volume commercial code, Fluent 6.3, is used. A pressure-based segregated solution algorithm, SIMPLE (Patankar & Spalding 1972) is employed. The second-order implicit time discretization scheme together with the second-order upwind space discretization for convective terms is chosen. No turbulence modelling is applied. For each simulation, initially a steady flow solution is performed with an unexcited fully developed turbulent velocity profile $u(y, t) = u(y)$ which has an average velocity of U. These inlet velocity profiles are determined through Reynolds-averaged Navier–Stokes (RANS) simulations at a Reynolds number of 5×10^4 for each different pipe diameter (D_p). The iterations are continued until all the residuals drop below 10^{-12}. Then, a velocity perturbation $u'(t)$ with a frequency (f) and an amplitude ($|u'|/U$),

$$u'(t) = \frac{|u'|}{U} \sin(2\pi f t), \tag{3.1}$$

is superposed on the inlet velocity profile ($u(y, t) = u(y) + u'(t)$), where $|u'|$ is the amplitude of the acoustic velocity induced by the longitudinal standing wave at the position of the cavity considered. This amplitude can be much lower than $|u'_{max}|$, if the cavity considered is close to a velocity node of the standing wave. The outlet boundary condition $\partial u_x / \partial x = 0$ is used. After checking different computation times, a typical time of 5 periods of the excitation frequency appeared to be sufficient; simulations with longer computation times provide the same results. The time step size is chosen as $\Delta t = 0.01 W/U$.

The computational domain contains approximately 70 000 quadrilateral cells which are clustered close to the opening of the cavity and to the walls, where there are high gradients of velocity due to shear layer and boundary layer, respectively. In the domain between $6W$ and $9W$ downstream of the cavity, shown as sponge zone in figure 11, cells with high aspect ratio ($\Delta x / \Delta y \gg 1$) are employed. By doing so, problems that can arise due to reverse flow at the outlet boundary condition are minimized. A study on mesh dependence has been carried out. The same computation was performed with 2 times and 4 times more densely meshed domains, producing differences in the calculated acoustic source power of less than 5 %.

3.2. Calculation of acoustic source power

Using the theory of vortex sound, the strength of the acoustic source for high-Reynolds-number flows is calculated from enthalpy differences, which are acquired from relatively low-Reynolds-number simulations ($Re = O(10^3)$). This is achieved by means of an extrapolation method. The effect of friction on the enthalpy losses is estimated by considering a reference flow through a straight smooth pipe (without a cavity). In this subsection, this approach is explained in detail.

The acoustic field can be defined by using a Helmholtz decomposition of the flow field $\boldsymbol{u}$, as proposed by Howe (1980):

$$\boldsymbol{u} = \nabla(\phi_0 + \phi') + \nabla \times \boldsymbol{\Psi}, \tag{3.2}$$

where $\boldsymbol{\Psi}$ is the streamfunction, ϕ_0 and ϕ' are the steady and unsteady components of the scalar potential, respectively. Recognizing that the solenoidal vector field is incompressible $\nabla \cdot (\nabla \times \boldsymbol{\Psi}) = 0$, the acoustic field corresponds to the unsteady potential component of the flow $\nabla \phi'$, which is compressible. The acoustical flow velocity ($\boldsymbol{u}'$) is defined by Howe (1980) as

$$\boldsymbol{u}' = \nabla \phi'. \tag{3.3}$$

For a subsonic flow with sufficiently high Reynolds number, the effect of friction can be neglected in the bulk of the flow. Assuming a homentropic flow, the momentum equation (Crocco's equation) can be written as follows:

$$\nabla B = -\frac{\partial \boldsymbol{u}}{\partial t} - \boldsymbol{\omega} \times \boldsymbol{u}, \tag{3.4}$$

where $\boldsymbol{\omega} = \nabla \times \boldsymbol{u}$ is the vorticity and B is the total enthalpy:

$$B = \tfrac{1}{2}|\boldsymbol{u}|^2 + i, \tag{3.5}$$

where i is the specific enthalpy. Here, it can be noted that the first term on the right-hand side of the momentum equation (3.4) is related to the potential flow solution and the second term corresponds to the Coriolis force density, $\boldsymbol{f}_c = -\rho(\boldsymbol{\omega} \times \boldsymbol{u})$, experienced by an observer moving with the flow velocity ($\boldsymbol{u}$). The latter is interpreted as the source of the sound.

Using the energy corollary of Howe (1998), the time-averaged acoustic source power $\langle P_{source} \rangle$ due to the Coriolis force can be estimated for low Mach number flows as follows:

$$\langle P_{source} \rangle = -\rho \left\langle \int_V (\boldsymbol{\omega} \times \boldsymbol{u}) \cdot \boldsymbol{u}' \, \mathrm{d}V \right\rangle, \tag{3.6}$$

where V is the volume in which $\boldsymbol{\omega}$ is non-vanishing and $\langle \cdot \rangle$ denotes the time averaging. Combining (3.6) with (3.4), $\langle P_{source} \rangle$ can be determined as follows:

$$\langle P_{source} \rangle = \rho \left\langle \int_V \nabla B' \cdot \boldsymbol{u}' \, \mathrm{d}V \right\rangle + \rho \left\langle \int_V \frac{\partial \boldsymbol{u}}{\partial t} \cdot \boldsymbol{u}' \, \mathrm{d}V \right\rangle, \tag{3.7}$$

where B' is the fluctuating total enthalpy. Knowing that in a compact source region, $\nabla \cdot \boldsymbol{u}'$ is negligibly small, the source term $\nabla B' \cdot \boldsymbol{u}'$ can be replaced by $\nabla \cdot (\boldsymbol{u}' B')$. Neglecting the contribution of the second integral in (3.7) and using the divergence theorem, $\langle P_{source} \rangle$ reads as

$$\langle P_{source} \rangle = \rho \left\langle \int_S (B' \boldsymbol{u}') \cdot \boldsymbol{n} \, \mathrm{d}S \right\rangle. \tag{3.8}$$

It is seen from (3.8) that the acoustic source power generated in a control volume can be calculated through the surface integral of fluctuating total enthalpy over the boundary of the control volume.

In this derivation, attention should be drawn to two points. Firstly, it is assumed in the momentum equation (3.4) that the effect of friction in the bulk of the fluid is small enough to be neglected. Secondly, it is assumed that the second integral in (3.7) has no contribution to the sound generation. The same conclusion can be deduced using as starting point the exact energy corollary of Myers (1986, 1991):

$$\langle P_{source} \rangle = \left\langle \int_S (B' \boldsymbol{m}') \cdot \boldsymbol{n} \, \mathrm{d}S \right\rangle, \tag{3.9}$$

where

$$B' = \frac{p'}{\rho} + \boldsymbol{u}_0 \cdot (\boldsymbol{u}' + \boldsymbol{u}'_h), \quad \boldsymbol{m}' = \rho(\boldsymbol{u}' + \boldsymbol{u}'_h) + \rho' \boldsymbol{u}_0,$$

where $\boldsymbol{u}_0$ is the time-averaged velocity and the fluctuations are split into the acoustical (potential) part $\boldsymbol{u}'$ and the hydrodynamical (rotational) part $\boldsymbol{u}'_h$. When ρ' is neglected (in agreement with the use of an incompressible flow model) and the contribution of the hydrodynamic velocity fluctuations ($\boldsymbol{u}'_h$) to the integral is also neglected, (3.8) is recovered. The contribution of the hydrodynamic velocity fluctuations is expected to depend on the spatial location of the control surface. It has been verified that by choosing a large enough control volume, such a dependence can be avoided.

The recent study of Martínez-Lera *et al.* (2009) has shown that after the time averaging, what they called the potential term, the second integral in (3.7) could still have a non-zero contribution to $\langle P_{source} \rangle$. These authors concluded that it is essential to remove the term $(-\partial \boldsymbol{u}/\partial t)$ from the enthalpy difference ($\Delta B'$) before taking the time averaging. Their technique is based on successive linear least-squares fits of the total pressure jumps considering many measuring planes both upstream and downstream of the cavity. This procedure provides promising results. However, the drawback is that the bounds of the source region cannot be determined. Because of the uncertainty in the spatial linear fit, $\langle P_{source} \rangle$ appears to depend significantly on the arbitrary choice of the position of the measuring planes. This is an indication that this approach is not able to completely remove the contribution of the hydrodynamic velocity fluctuations to the source power.

Here an alternative method is proposed in which the contribution of hydrodynamic velocity fluctuations is effectively removed from the source power. This is done by means of a reference flow simulation in a straight pipe with identical boundary conditions with the respective cavity simulation and using the same measurement
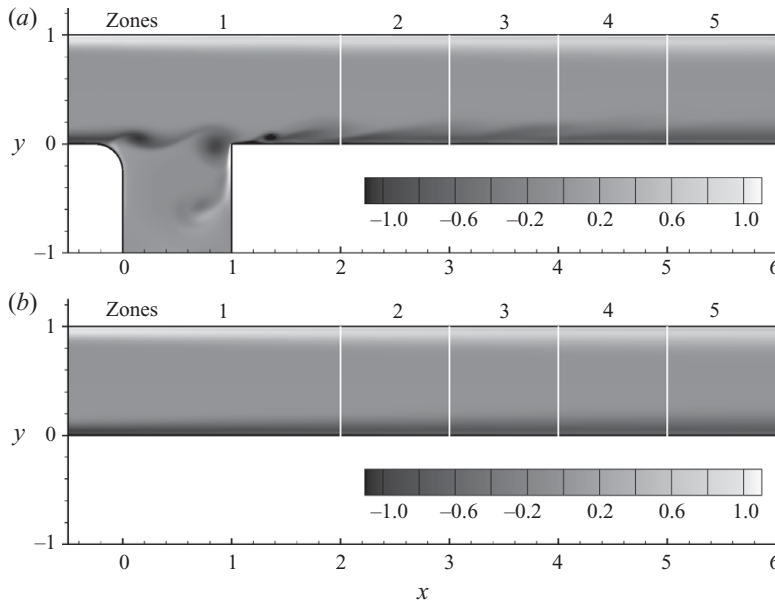
FIGURE 12. Normalized vorticity contours for (*a*) a confined cavity flow and (*b*) a reference flow in a straight pipe ($Re = 4000$, $Sr = 0.6$ and $|u'|/U = 0.2$). White lines represent the measurement sections where area-averaged total enthalpy is recorded.

sections in the duct. Then, $\langle P_{source} \rangle$ between any two measurement sections located at x_1 and x_2 in the duct, which e.g. correspond to two vertical white lines in figure 12, can be estimated as follows:

$$\langle P_{source} \rangle = \rho \left\langle \frac{1}{4} \left[\left(B'_{x_2} - B'_{x_1} \right)_{cav} - \left(B'_{x_2} - B'_{x_1} \right)_{ref} \right] u' \pi D_p^2 \right\rangle. \tag{3.10}$$

The proposed approach is an extrapolation method for high-Reynolds-number flows, in which the solution is expected to be Reynolds number independent. For a simulation with a perturbation amplitude of $|u'|/U = 0.1$, from figure 13 it is seen that calculated average acoustic source powers are converging to a Reynolds number independent limit.

Other simulations that are considered here have also similar characteristics in which above a certain Reynolds number $\langle P_{source} \rangle$ can be assumed to weakly depend on the Reynolds number. Within the accuracy of the proposed approach (5 %), this limit is determined as $Re = 4000$, which is used in all the simulations. By increasing the number of cells in the computational domain, simulations with higher Reynolds numbers can be achieved, which will increase the Reynolds number independence of the results.

Using this approach, the extent of the source region in the duct can be determined. All the numerical simulations independent of the Strouhal number and perturbation amplitude have a similar bound for the source region, which is between $0.5W$ upstream of the cavity and W downstream of the cavity, shown as zone 1 in figure 12. Note that $\langle P_{source} \rangle$ remains constant within 5 % when the bounds of the control volume are extended to include zones 2–4. In some calculations, the reference flow solution for smooth pipes is carried out with a slip boundary condition for the section of the
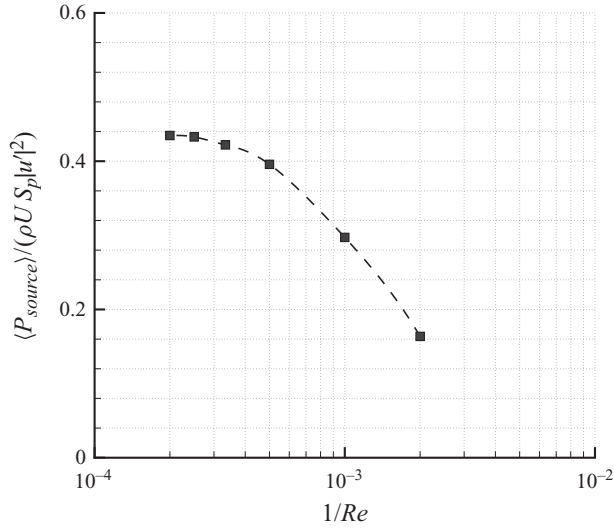
FIGURE 13. Convergence to high-Reynolds-number limit: $1/Re$ is plotted against dimensionless average acoustic source power $\langle P_{source}\rangle/(\rho U S_p|u'|^2)$ for $D_p/W = 2$ and $|u'|/U = 0.1$.
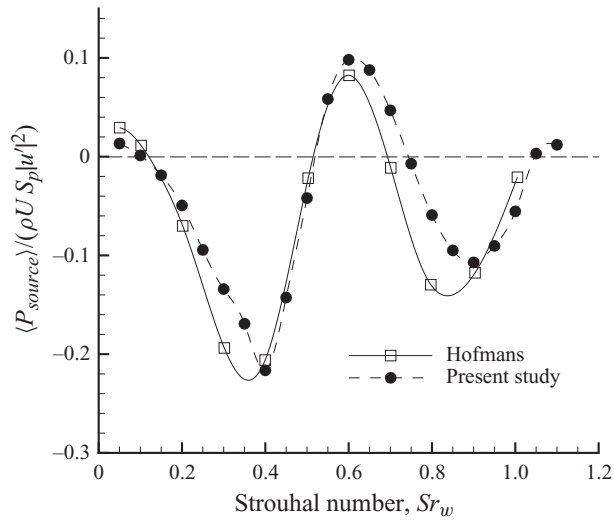

FIGURE 14. Strouhal number plotted against dimensionless average acoustic source power $\langle P_{source}\rangle/(\rho U S_p|u'|^2)$ for a cavity (present study) and a T-joint (Hofmans 1998) with $r_{up}/W = 0$ and $|u'|/U = 0.2$.

wall which corresponds to the cavity location. The results are almost identical to the results presented here.

Simulations have been performed to check the capability of the proposed approach in predicting the Strouhal number range where there is sound production. In figure 14, the dimensionless average acoustic source power $\langle P_{source}\rangle/(\rho U S_p|u'|^2)$ is displayed as a function of the Strouhal number for a cavity with sharp edges and for a perturbation amplitude of $|u'|/U = 0.2$. The results are presented together with the data obtained by Hofmans (1998), using an inviscid two-dimensional vortex blob method for a

T-joint with the same geometry and perturbation amplitude for a configuration similar to corrugated pipes, where there is a grazing flow in the main pipe. Two ranges of the Strouhal number with positive dimensionless average acoustic source power are distinguished where there is sound production. The lower ($Sr_W < 0.1$) and the higher ($0.52 < Sr_W < 0.74$) Strouhal number ranges correspond to the first and second hydrodynamic modes, respectively. In the first hydrodynamic mode, there exists a single vortex in the cavity mouth and the travelling time of the vortex across the opening is 0.25 oscillation period. However, for the second hydrodynamic mode, two vortices are present at the same moment in the cavity mouth. A vortex takes 1.25 oscillation periods to travel across the cavity (Bruggeman *et al.* 1991). It is clear that the second hydrodynamic mode is stronger than the first one, explaining why the experimentally observed peak-whistling Strouhal numbers belong to the second hydrodynamic mode. Acoustic source powers predicted by the present methodology are in agreement with the data of Hofmans (1998). A peak-whistling Strouhal number $Sr_{p\text{-}w}$ of 0.6 is estimated. This is close to the experimental observation with multiple side branch systems, which is $Sr_{p\text{-}w} = 0.62 \pm 0.02$ (figure 9). The peak-whistling Strouhal number is further discussed in §3.4.

3.3. *Nonlinear saturation of the shear layer*

The aeroacoustic behaviour of corrugated pipes and the multiple side branch system depends strongly on the perturbation amplitude, $|u'|/U$. At low perturbation amplitudes, the instability of the shear layer can be described by the linear-stability theory (Rayleigh 1945), in which the acoustic source power $\langle P_{source} \rangle$ grows quadratically with perturbation amplitude (Bruggeman *et al.* 1991). In this regime, the vorticity disturbances are amplified by a factor $e^{2\pi}$ over one hydrodynamic wavelength in the shear layer (Bruggeman, Wijnands & Gorter 1986). For the second hydrodynamic mode, this corresponds to an amplification of $e^{5\pi/2} \approx 2.6 \times 10^3$. Evidently, this imposes a perturbation amplitude limit of around 10^{-3} to the validity of the linear theory above which nonlinearities become essential (Tam & Block 1978). In this range, the amplitude of the oscillations is determined by nonlinearities, such as roll-up of the shear layer into discrete vortices (Fletcher 1979; Keller 1984; Bruggeman *et al.* 1991; Rowley *et al.* 2006).

The proposed approach predicts the linear range and the nonlinear saturation of the shear layer, as demonstrated in figure 15 for a simulation with $D_p/(W + r_{up}) = 3.2$. For small perturbation amplitudes $|u'|/U \leqslant 10^{-3}$, the shear layer behaves linearly. Therefore, the acoustic source power grows quadratically with $|u'|/U$, making the dimensionless average acoustic source power $\langle P_{source} \rangle / (\rho U S_p |u'|^2)$ constant. Eventually, around $|u'|/U \approx 10^{-2}$, nonlinearities become dominant and $\langle P_{source} \rangle / (\rho U S_p |u'|^2)$ starts to decrease with $|u'|/U$.

This amplitude-dependence test of $\langle P_{source} \rangle$ is performed for Strouhal numbers of 0.5, 0.56 and 0.63. Similar to the simulations discussed in the previous section, initial simulations have been performed at a constant perturbation amplitude $|u'|/U$ with various Strouhal numbers to determine the peak-whistling Strouhal number for a confinement ratio of $D_p/(W + r_{up}) = 3.2$. The peak-whistling Strouhal number $St_{p\text{-}w}$ is estimated as 0.56. Then, two other Strouhal numbers close to the peak-whistling Strouhal number are also studied to investigate whether there is a dependence of the peak-whistling Strouhal number on perturbation amplitude. From figure 15, it is seen that the peak-whistling Strouhal number does not alter significantly with the perturbation amplitude.
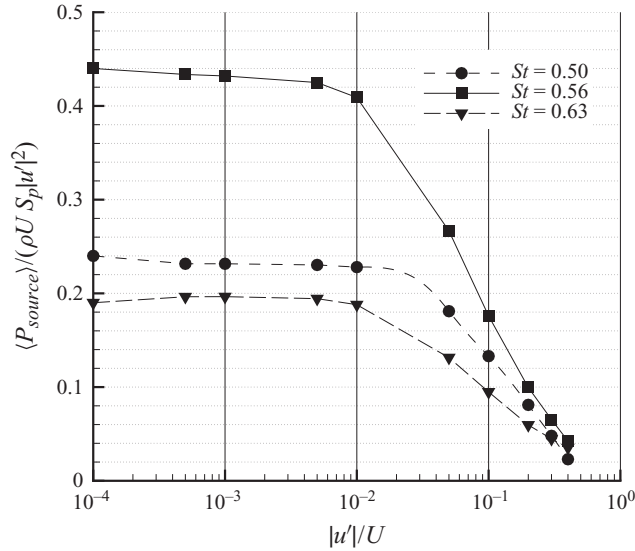
FIGURE 15. Perturbation amplitude $|u'|/U$ plotted against dimensionless average acoustic source power $\langle P_{source}\rangle/(\rho U S_p |u'|^2)$ for $D_p/(W + r_{up}) = 3.2$ and for Strouhal numbers of 0.5, 0.56 and 0.63.

3.4. Peak-whistling Strouhal number difference in periodic systems

Previous studies on whistling periodic systems have shown that there is a difference in peak-whistling Strouhal numbers between multiple side branch systems and corrugated pipes (Nakiboğlu *et al.* 2010; Tonon *et al.* 2010). As demonstrated in figure 10, the peak-whistling Strouhal number in multiple side branch systems $Sr_{p\text{-}w} = 0.62$ is higher than those observed in most corrugated pipes $0.3 < Sr_{p\text{-}w} < 0.6$. To investigate the reason for this variation in $Sr_{p\text{-}w}$, two sets of simulations have been performed. In multiple side branch system simulations, a 2D domain is used with a confinement ratio of $D_p/(W + r_{up}) = 0.8$, close to the experimental value. For corrugated pipe simulations, a cylindrical symmetric 2D domain is used to mimic a circumferential cavity. Also, a larger confinement ratio is chosen for corrugated pipe simulations $D_p/(W + r_{up}) = 3.2$. Taking the confinement ratio of actual corrugated pipes $2 \leqslant D_p/(W + r_{up}) \leqslant 30$ (see table 1) into account, the pipe that is simulated has a rather small confinement ratio. In both sets of simulations, a perturbation amplitude $|u'|/U$ of 0.05 is used. This particular perturbation amplitude is a typical fluctuation amplitude observed in experiments, as shown in figures 6–9 (Belfroid *et al.* 2007; Nakiboğlu *et al.* 2010). The results for these two set of simulations are presented in figure 16. In parallel with the experimental data, for the multiple side branch system a higher peak-whistling Strouhal number $Sr_{p\text{-}w} = 0.65$ is observed than for the corrugated pipe $Sr_{p\text{-}w} = 0.55$. Although these simulations show that the proposed numerical approach can predict the difference in peak-whistling Strouhal numbers between these two periodic systems, the reason for this difference remains unexplained.

As discussed in §2.6, experiments indicate that there is a dependence of the peak-whistling Strouhal number on the confinement ratio $D_p/(W + r_{up})$. To address this effect of confinement, three sets of numerical simulations have been performed, which correspond to the experiments of Binnie (1961). The result of the first set
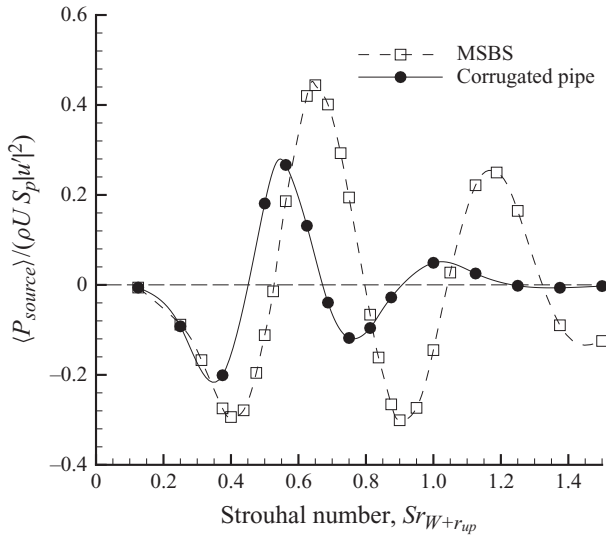
FIGURE 16. Strouhal number plotted against dimensionless average acoustic source power $\langle P_{source}\rangle/(\rho U S_p |u'|^2)$ for a multiple side branch system with a confinement ratio of $D_p/(W + r_{up}) = 0.8$ and for a corrugated pipe with a confinement ratio of $D_p/(W + r_{up}) = 3.2$ ($|u'|/U = 0.05$).

of simulations is presented in figure 16, where a cavity in a cylindrical symmetric configuration is solved for a $D_p/(W + r_{up})$ ratio of 3.2. In the other two sets of simulations, the same cylindrical symmetric domain is used together with rods of diameter $D_r = 2W$ or $D_r = 3W$ respectively, which are placed coaxially inside the pipe to vary the confinement ratio. As explained in § 2.6, in the presence of a rod, the confinement ratio is defined as $(D_p - D_r)/(W + r_{up})$. The dimensionless average acoustic source power $\langle P_{source}\rangle/(\rho U S_p |u'|^2)$ for these configurations is presented as a function of the Strouhal number in figure 17. It is seen that in accordance with the experimental observations, as the confinement ratio decreases, the peak-whistling Strouhal number increases. For confinement ratios $(D_p - D_r)/(W + r_{up})$ of 3.2, 1.6 and 0.8, peak-whistling Strouhal numbers $Sr_{p\text{-}w}$ of 0.55, 0.67 and 0.73 are estimated, respectively.

Ziada & Shine (1999) explained the shift in the peak-whistling Strouhal number by a change in the velocity profile. To investigate this argument, the same sets of simulations that are presented in figure 17 are repeated. But instead of using a fully developed turbulent velocity profile, in all the simulations the same boundary layer profile as used by Martínez-Lera *et al.* (2009) is considered: a uniform velocity profile in the core of the flow with a boundary layer of momentum thickness $\theta = 0.0065 D_p$. The momentum thickness (Eggels *et al.* 1994) is defined here as

$$\theta(D_p - \theta) = 2 \int_0^{D_p/2} r \frac{u(r)}{U_0}\left(1 - \frac{u(r)}{U_0}\right) \mathrm{d}r, \tag{3.11}$$

where $u(r)$ is the radial profile of the axial velocity, U_0 is the velocity at the centreline of the duct, and for coordinates see figure 11. The dimensionless average acoustic source powers $\langle P_{source}\rangle/(\rho U S_p |u'|^2)$ for these three configurations are presented as a function of the Strouhal number in figure 18. It is seen that the peak-whistling Strouhal number $Sr_{p\text{-}w} = 0.68$ remains constant with changing confinement ratio $(D_p - D_r)/(W + r_{up})$, if
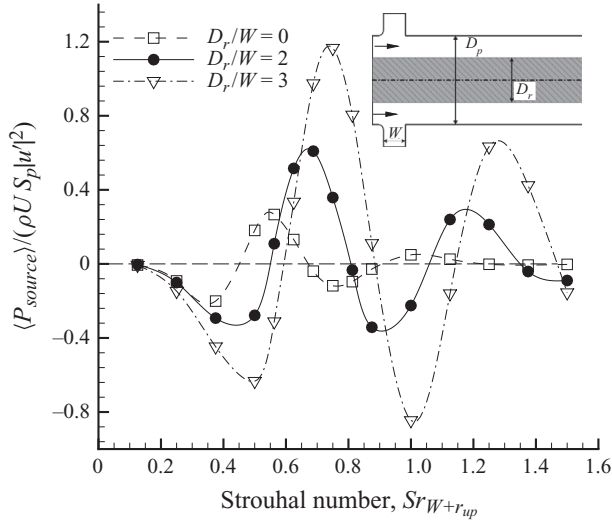
FIGURE 17. Strouhal number plotted against the dimensionless average acoustic source power $\langle P_{source}\rangle/(\rho U S_p |u'|^2)$ for a corrugated pipe with $D_p/(W + r_{up}) = 3.2$ and for rod diameters of $D_r/W = 0$, $D_r/W = 2$ and $D_r/W = 3$; $|u'|/U = 0.05$, $\theta/D_p = 3 \times 10^{-2}$.
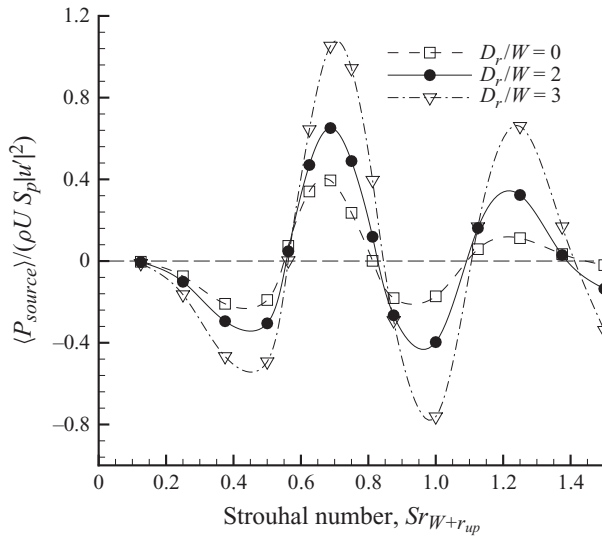

FIGURE 18. Strouhal number plotted against the dimensionless average acoustic source power $\langle P_{source}\rangle/(\rho U S_p |u'|^2)$ for a corrugated pipe with $D_p/(W + r_{up}) = 3.2$ and for rod diameters of $D_r/W = 0$, $D_r/W = 2$ and $D_r/W = 3$. Same approach velocity profile (3.11) is used in all simulations; $r_{up}/W = 0.25$, $|u'|/U = 0.05$, $\theta/D_p = 6.5 \times 10^{-3}$.

the same velocity profile is used at the inlet. Thus, in agreement with the interpretation of Ziada & Shine (1999), the shift observed in the peak-whistling Strouhal number can be attributed to a change in the velocity profile due to an alteration in the confinement ratio, rather than a pure confinement effect.

To evaluate the capability of the proposed numerical approach in predicting the peak-whistling Strouhal number, simulations with larger confinement ratios are also
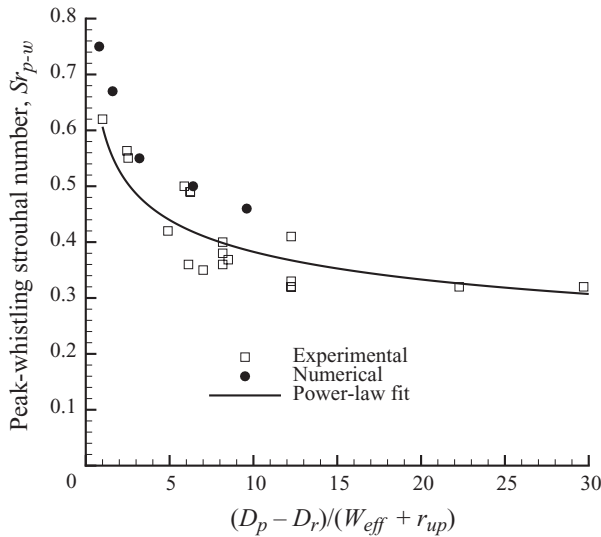
FIGURE 19. Measured and estimated peak-whistling Strouhal numbers plotted against confinement ratio together with the proposed formula,
$St_{p\text{-}w} = 0.58[(D_p - D_r)/(W_{eff} + r_{up})]^{-0.2}$.

carried out. In figure 19, the available experimental data (figure 10) are compared with the numerical estimations. Although estimated peak-whistling Strouhal numbers are somewhat larger than the measured values, using the proposed numerical approach, the dependence of the peak-whistling Strouhal number on the confinement ratio is successfully captured.

For grazing flows along wall-mounted cavities in the presence of turbulent boundary layers, a dependence of the convection velocity of shear-layer perturbations (U_c) on the non-dimensional boundary-layer thickness ($\Gamma = \delta/W$) has been reported by Elder, Farabee & DeMetz (1982). Later, for orifices subjected to a grazing turbulent boundary-layer flow, Golliard (2002) proposed an empirical formula for the convection velocity as a function of non-dimensional boundary-layer thickness as follows:

$$\frac{U_c}{U_\infty} = 0.4\Gamma^{-0.2}, \tag{3.12}$$

where U_∞ is the free-stream velocity. Associating the convection velocity (Kooijman, Hirschberg & Golliard 2008), the peak-whistling Strouhal number can be stated as follows:

$$St_{p\text{-}w} = \left(\frac{f(W_{eff} + r_{up})}{U_c}\right)\left(\frac{U_0}{U}\right)\left(\frac{U_c}{U_0}\right), \tag{3.13}$$

Here, $(W_{eff} + r_{up})/U_c$ is the time that it takes a vortex to cross the cavity mouth, which is 1.25 oscillation periods for the second hydrodynamic mode (Bruggeman *et al.* 1991). The second term is the ratio of maximum velocity (U_0) to the average velocity (U) in the duct, which is taken as 1.23, considering the fully developed turbulent profiles ($Re = 5 \times 10^4$) used in the simulations (Schlichting 1979). For the last term, an empirical formula similar to (3.12) is employed. The free-stream velocity (U_∞) and the dimensionless boundary-layer thickness (Γ) are replaced by the maximum velocity in the duct ($U_\infty = U_0$) and the confinement ratio ($\Gamma = (D_p - D_r)/(W + r_{up})$), respectively. Finally, an empirical formula for the peak-whistling Strouhal number as
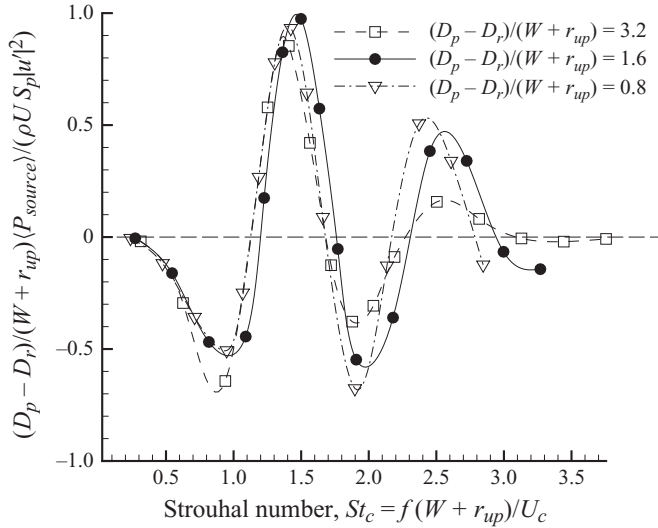
FIGURE 20. Strouhal number based on the convective velocity $St_c = f(W + r_{up})/U_c$ plotted against the normalized dimensionless average acoustic source power $(D_p - D_r)/(W + r_{up})$ $\langle P_{source}\rangle/(\rho U S_p |u'|^2)$ for confinement ratios $(D_p - D_r)/(W + r_{up})$ of 3.2, 1.6 and 0.8.

a function of the confinement ratio is obtained for fully turbulent flows as

$$St_{p\text{-}w} = 0.63 \left(\frac{D_p - D_r}{W + r_{up}} \right)^{-0.2}. \tag{3.14}$$

A power-law fit of the experimental data yields 0.58 instead of 0.63, which is shown in figure 19. It is seen that this rather simple empirical formula explains the broad range of peak-whistling Strouhal numbers observed in periodic systems as an effect of changing velocity profile due to changing confinement ratio.

3.5. *Time-averaged acoustic source power in periodic systems*

Up to now attention has been given to the peak-whistling Strouhal number. In this section, the time-averaged acoustic source power in periodic systems is addressed. From figure 17, it is seen that the non-dimensional acoustic source power $\langle P_{source}\rangle/(\rho U S_p |u'|^2)$ decreases almost linearly with increasing confinement ratio $((D_p - D_r)/(W + r_{up}))$ for the second hydrodynamic mode. Thus, if the non-dimensional averaged acoustic source power is normalized with the confinement ratio as $(D_p - D_r)/(W + r_{up})\langle P_{source}\rangle/(\rho U S_p |u'|^2)$, then a universal graph of the source power for periodic systems with various confinement ratios can be obtained. In figure 20, the normalized non-dimensional average acoustic source power is shown as a function of the Strouhal number based on the convection velocity $(St_c = f(W + r_{up})/U_c)$. Considering the convection velocity U_c, instead of the mean flow velocity U in the Strouhal number definition, collapses the peak-whistling Strouhal numbers into a single peak $(St_c = 1.4)$. From figure 20, it is seen that for the third hydrodynamic mode $(St_c = 2.5)$ as the confinement ratio increases, the normalized dimensionless averaged acoustic source power decreases. This decrease could be explained on the basis of the linear theory of Michalke (1965) on the effect of finite momentum thickness (θ) on the spatial amplification of the shear-layer instability. Following the theory, above a critical value of $f\theta/U = 0.04$, the amplification vanishes (Bruggeman *et al.* 1991). It should be noted that the third hydrodynamic mode has not been

reported in any experimental study on corrugated pipes. It is therefore difficult to verify this result. Another consequence of the theory is that (3.14) has a limited range of validity. Above a critical ratio of D_p/W whistling will not occur also for the second hydrodynamic mode.

3.6. *Estimation of the pressure fluctuation amplitude in a periodic system*

To estimate the amplitude of self-sustained oscillations, i.e. whistling, in a periodic system an energy balance model is required, where the acoustic sources and the acoustic losses are equalized:

$$\langle P_{source} \rangle = \langle P_{visc} \rangle + \langle P_{conv} \rangle + \langle P_{rad} \rangle, \tag{3.15}$$

where $\langle P_{source} \rangle$ is the time-averaged acoustic source power, $\langle P_{visc} \rangle$, $\langle P_{conv} \rangle$ and $\langle P_{rad} \rangle$ are the time-averaged power losses due to visco-thermal, convective and radiation effects, respectively. In contrast to the acoustic sources which are calculated spatially locally as explained in §3, acoustic losses are estimated for the whole system. Here, first the estimation of acoustic losses is considered (Tonon *et al.* 2010) and then the prediction of pressure fluctuation amplitudes is discussed for two periodic systems, namely a corrugated segment in a smooth pipe and a unit length of a long corrugated pipe.

In order to calculate the acoustic power dissipated by the visco-thermal damping of acoustic waves in a periodic system, a standing wave built up of right p^+ and left p^- travelling waves of equal amplitude is assumed. Then, the visco-thermal losses are given by

$$\frac{\langle P_{visc} \rangle}{\rho U S_p |u'_{max}|^2} = \frac{1}{2} \frac{c_0^2 \alpha L_p}{c_{eff} U}, \tag{3.16}$$

where c_0 is the speed of sound, c_{eff} is the effective speed of sound in the pipe, L_p is the pipe length and α is the acoustic damping coefficient. Note that here the acoustic losses are non-dimensionalized by the use of $|u'_{max}|$ instead of $|u'|$ because the global behaviour of the standing wave is considered.

To determine the acoustic losses due to convective effects, vortex shedding at the downstream pipe termination is considered. Instead of describing the flow in detail, a quasi-steady free jet formed at the outlet of the pipe is assumed. Using the acoustic energy reflection coefficient of Ingard & Singhal (1975) and assuming the incompressible limit, the acoustic power loss due to vortex shedding at the outlet of the system is determined as follows:

$$\frac{\langle P_{conv} \rangle}{\rho U S_p |u'_{max}|^2} = \frac{1}{2} \frac{c_0}{c_{eff}}. \tag{3.17}$$

It should be noted that this approximation is limited to low frequencies. At high frequencies, the approximation proposed by Munt (1977, 1990) should be used (Peters *et al.* 1993).

Furthermore, compared with the acoustic losses due to visco-thermal dissipation and convective effects, the radiation losses at the pipe terminations are rather small. Thus, they are neglected in the calculations.

3.6.1. *A corrugated segment in a smooth pipe*

A corrugated segment in a smooth pipe is technologically useful as it allows bending the pipe. When appropriately designed it should not whistle. Elliott (2005) performed tests with a corrugated segment composed of 10 corrugations in a smooth pipe as shown in figure 21. The pipe has a length (L_p) of 1031 mm and an inner diameter
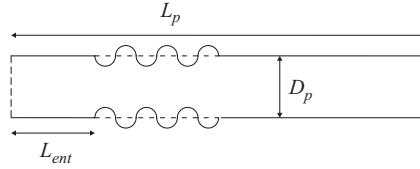
FIGURE 21. A corrugated segment in a smooth pipe as described by Elliott (2005).

(D_p) of 10.65 mm. The pitch length of corrugations is $Pt = 2.13$ mm. Unfortunately, r_{up} is not explicitly mentioned by Elliott (2005). Thus, r_{up} is taken as $0.25W$, which is a typical value for this type of corrugated pipe (see figure 2b), which leads to a confinement ratio of $D_p/(W + r_{up}) = 5.8$. It is reported that when the corrugated segment is placed at the beginning of the pipe, $L_{ent} = 0$, the system just whistles at $U = 8.6$ m s^{-1} with a frequency of 1488 Hz, which corresponds to the ninth axial mode.

Since the corrugated segment is 21.3 mm, which is only 2 % of the total pipe length, when calculating $\langle P_{visc} \rangle$ and $\langle P_{conv} \rangle$, the effective speed of sound c_{eff} is taken equal to the speed of sound c_0. For the same reason, the theory of Kirchhoff (Pierce 1981; Peters *et al.* 1993) for smooth pipes is used to estimate the damping coefficient α, as follows:

$$\alpha = \frac{L_{per}}{2S_p c_0} \sqrt{\frac{\pi f \mu}{\rho}} \left(1 + \frac{c_p/c_v - 1}{\sqrt{Pr}} \right), \tag{3.18}$$

where L_{per} is the perimeter of the pipe, f is the sound wave frequency, μ is the dynamic viscosity, c_p/c_v is the ratio of specific heat capacities and Pr is the Prandtl number. Then, using (3.16) and (3.17) the total acoustic loss is determined as $(D_p/(W + r_{up}))\langle P_{loss} \rangle/(\rho U S_p |u'_{max}|^2) = 28.4$. Here, the interaction between the acoustic boundary layer and the turbulent main flow is neglected. This is justified by the relatively low Reynolds numbers prevailing in the experiments (Peters *et al.* 1993; Howe 1998).

To estimate the source power of the system, first the location of the corrugated segment with respect to the standing wave should be determined. The average acoustic source power of a corrugation presented in figure 15 is valid only for cavities that are located in the vicinity of pressure nodes of the standing wave, where the sound production is maximum. Considering the fact that the system whistles at the ninth acoustic mode, the wavelength of the standing wave pattern is approximately $\lambda = 230$ mm. Thus, compared with the wavelength, a segment of 21.3 mm at the beginning of the pipe is small enough to assume that all the corrugations are close to the pressure node.

In figure 22, the normalized dimensionless average acoustic source power is presented as a function of the perturbation amplitude for a fully developed turbulent velocity profile and a thin boundary-layer velocity profile (3.11). The proposed model predicts whistling with 15 corrugations instead of 10 corrugations, as found in the experiments. The acoustic loss per corrugation, $(D_p/(W + r_{up}))\langle P_{source} \rangle/(\rho U S_p |u'_{max}|^2) = 1.89$, is indicated by a horizontal line in figure 22 (acoustic losses – corrugated segment) and the respective predicted amplitude $|u'_{max}|/U = 1.1 \times 10^{-2}$ by a vertical line. It should be noted that since the corrugated segment is located at the beginning of the pipe, the velocity profile is not yet developed. Consequently, the source calculated for a thin boundary layer is used to predict the whistling and its amplitude.
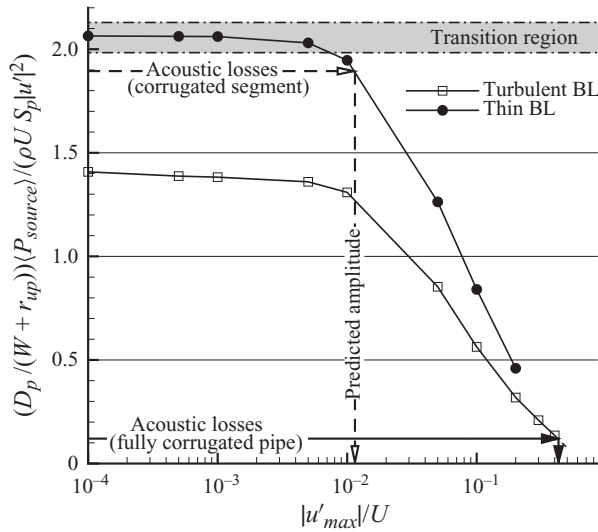
FIGURE 22. Maximum perturbation amplitude $|u'_{max}|/U$ is plotted against the normalized dimensionless average acoustic source power $(D_p/(W + r_{up}))\langle P_{source}\rangle/(\rho U S_p|u'|^2)$ for a fully developed turbulent velocity profile (turbulent BL) and a thin boundary-layer velocity profile (thin BL).

Elliott (2005) reported that when the corrugated segment is shifted such that $L_{ent} > 100$ mm, no oscillations could be produced. This can be explained by the change of the velocity profile upstream from the corrugated segment. When the corrugated segment is shifted such that $L_{ent} > 10D_p$, instead of a thin boundary-layer profile, a developed turbulent velocity profile will enter the corrugated segment. As shown in figure 22, the normalized dimensionless average acoustic source power is much smaller for the fully developed turbulent velocity profile than for the thin boundary-layer velocity profile. Consequently, the system which is just whistling for $L_{ent} = 0$ stops whistling when it is shifted to the next pressure node of the standing wave.

Figure 22 also indicates that in the transition region ($10^{-3} < |u'_{max}|/U < 10^{-2}$), a small increase in the acoustic losses can suppress the whistling. As a result, it is difficult to predict whistling in this amplitude zone.

3.6.2. *A fully corrugated pipe*

In this section, the whistling amplitude for a long corrugated pipe is estimated for a unit length. A typical corrugated pipe geometry (Com 3 in table 1) with a confinement ratio of $D_p/(W + r_{up}) = 5.9$ is used for the calculations. The pitch length of the corrugations is $Pt = 10$ mm, meaning that there are 100 corrugations in a unit length segment. For systems with such a high number of cavities, it can be assumed that the cavities are uniformly distributed along the standing wave. Thus, to estimate the average acoustic sound production per cavity, the maximum acoustic sound production per cavity (see figure 22) should be multiplied by $(2/\pi)$, which is the average of the absolute value of a cosine function. This factor corresponds to the assumption of a moderate amplitude behaviour (Bruggeman *et al.* 1991; Tonon *et al.* 2010). This assumption is only reasonable for high oscillation amplitudes $|u'|/U > 0.05$. Since the pipe is long, it can also be assumed that the convective

losses are small compared with the viscous losses $\langle P_{conv}\rangle \ll \langle P_{visc}\rangle$, so that they can be neglected in (3.15).

As a first approximation, similar to the calculations in the previous section, the theory of Kirchhoff (3.18) is used to estimate the damping coefficient. Following (3.15) and (3.16), the normalized dimensionless acoustic loss per corrugation $(D_p/(W + r_{up}))\langle P_{source}\rangle/(\rho U S_p |u'_{max}|^2) = 2.8 \times 10^{-2}$ is determined. This leads to maximum perturbation amplitudes which are a factor 5 higher than the experimentally observed $|u'_{max}|/U = 0.1$.

As a second approach, assuming a quasi-steady flow (Ingard & Singhal 1975) and linearizing the pressure gradient, the fluctuating pressure drop is stated as follows:

$$\frac{\mathrm{d}p'}{\mathrm{d}x} = \rho U u'\frac{4c_f}{D_p}, \tag{3.19}$$

where c_f is the experimentally determined resistance coefficient. For the corrugated pipe investigated (Com 3 in table 1), $c_f \approx 0.025$. The damping coefficient for acoustic waves is given by

$$\alpha = \frac{U_0}{c_{eff}}\frac{4c_f}{D_p}. \tag{3.20}$$

Similarly, following (3.15) and (3.16), this approach leads to a maximum perturbation amplitude ($|u'_{max}|/U$) of 0.4, which is a factor 4 larger than the measured values (see figure 22, acoustic losses – fully corrugated pipe). However, it should be noticed that although the predicted fluctuation amplitude is fairly close to the experimental observations, this approach has a fundamental drawback. When calculating the source power $\langle P_{source}\rangle$, the losses due to flow separation at each cavity are implicitly included in the simulations. By introducing the experimentally measured resistance coefficient (c_f) to calculate the damping coefficient, this nonlinear effect is again taken into account in the quasi-steady approximation. Also, the model neglects heat transfer losses. Thus, some of the loss terms are overestimated and some are excluded in this prediction. Finally, it should be noted that a quasi-steady approach is only valid at very low frequencies.

3.7. Discussion

In this study, a methodology which combines incompressible numerical simulations and the theory of vortex sound is introduced to estimate the acoustic source power in periodic systems. A comparison with the experimental measurements and the earlier studies indicates that the proposed method is promising in many aspects for the physical understanding of the whistling behaviour of periodic systems. However, the methodology has certain limitations.

First of all, it is assumed that the cavities are only acoustically coupled. Thus, any hydrodynamic interaction between cavities is neglected. Derks & Hirschberg (2004) showed that hydrodynamic interaction can be important for Helmholtz resonators if the plateau length between successive openings is smaller than the opening width ($l \leqslant W$). Similarly, for corrugated pipes with short plateau lengths, hydrodynamic interaction is expected to play a role.

Secondly, the approach does not include any turbulence modelling. This puts a limit on the cavity depth to cavity width ratio (H/W) that can be studied with this method. For shallow cavities ($H/W \leqslant 0.5$), where turbulence plays a significant role (Gloerfelt 2009; Nakiboğlu et al. 2010), the approach is not applicable. However, most of the corrugated pipes used in industrial applications have deep cavities ($H/W \geqslant 0.5$).

Another point that can be improved is the inlet boundary condition for incompressible simulations. As demonstrated in §§ 3.4 and 3.6, the velocity profile is essential for both the peak-whistling Strouhal number and fluctuation amplitude. Instead of using a fully developed turbulent velocity profile for smooth pipes at the inlet boundary, for each corrugated pipe geometry, respective fully developed velocity profiles can be estimated using RANS calculations. Preliminary calculations using this approach indicate a shift in predicted peak-whistling Strouhal numbers towards the proposed empirical power-law formula (3.14). Such an approach, however, will also be limited because whistling at large amplitudes is expected to affect the main flow profile, which cannot be predicted by RANS simulations.

It should be noted that using the theory of Kirchhoff for the estimation of the damping coefficient leads to overpredicted fluctuation amplitudes in long corrugated pipes. The quasi-steady approximation is not a satisfactory alternative either. Further research is needed on the estimation of visco-thermal losses of acoustic waves propagating in corrugated pipes.

Our standing wave model is only reasonable when the resonator has a large quality factor. For the investigation of very long corrugated pipes, a travelling wave model could be employed rather than a standing wave model.

4. Conclusions

Experiments performed on corrugated pipe segments of various lengths and cavity geometries show that the peak-whistling Strouhal number, based on cavity width plus upstream edge radius as characteristic length, is independent of the pipe length.

The experiments on corrugated pipes revealed a saturation behaviour in the amplitude of the pressure fluctuation $|p'_{max}|/\rho c_0 U \approx 0.1$. Although the segment length, where this saturation level is reached, varies depending on the type of the corrugated pipe, the saturation amplitude remains about the same.

The broad range of peak-whistling Strouhal numbers in corrugated pipes, $0.3 \leqslant St_{p\text{-}w} \leqslant 0.6$, which has been reported in the literature, is observed experimentally. There is a decrease of the peak-whistling Strouhal number with increasing confinement ratio, which is defined as the ratio of pipe diameter to cavity width plus upstream edge radius $D_p/(W + r_{up})$.

The proposed numerical methodology predicts Strouhal number ranges of acoustic energy production and absorption, which are in agreement with earlier studies about periodic systems. The nonlinear saturation of the shear layer, responsible for the stabilization of the limit cycle oscillation, is also successfully captured with the current approach.

It is explained that the variation observed in the peak-whistling Strouhal number due to a change of confinement ratio results from a different main flow velocity profile. Assuming a fully developed turbulent velocity profile for a smooth channel flow at the inlet, the proposed methodology predicts the decrease of the peak-whistling Strouhal number with increasing confinement ratio. The estimated peak-whistling Strouhal numbers are in a reasonable agreement with the experimentally measured values. An empirical formula for the peak-whistling Strouhal number as a function of confinement ratio is proposed, which relates this effect to earlier observations from the literature on cavities (Elder *et al.* 1982; Golliard 2002; Kooijman *et al.* 2008) and deep resonant side branches (Ziada & Shine 1999).

Combined with an energy balance, the proposed model is used to explain qualitatively the difference observed in acoustic fluctuation amplitudes in periodic

systems due to variations of cavity geometry and flow parameters. However, it should be improved before being a quantitative tool for the prediction of the pulsation amplitude.

REFERENCES

ÅBOM, M. & BODÉN, H. 1988 Error analysis of two-microphone measurements in ducts with flow. *J. Acoust. Soc. Am.* **83**, 2429–2438.

BELFROID, S. P. C., SHATTO, D. P. & PETERS, R. M. 2007 *Flow Induced Pulsation Caused by Corrugated Tubes.* ASME Pressure Vessels and Piping Division, San Antonio, Texas.

BINNIE, A. M. 1960 Self-induced waves in a conduit with corrugated walls. I. Experiments with water in an open horizontal channel with vertically corrugated sides. *Proc. R. Soc. Lond.* A **259**, 18–27.

BINNIE, A. M. 1961 Self-induced waves in a conduit with corrugated walls. II. Experiments with air in corrugated and finned tubes. *Proc. R. Soc. Lond.* A **262**, 179–191.

BRUGGEMAN, J. C., HIRSCHBERG, A., VAN DONGEN, M. E. H., WIJNANDS, A. P. J. & GORTER, J. 1991 Self-sustained aero-acoustic pulsations in gas transport systems: experimental study of the influence of closed side branches. *J. Sound Vib.* **150**, 371–393.

BRUGGEMAN, J. C., WIJNANDS, P. J. & GORTER, J. 1986 Self-sustained low-frequency resonance in low-Mach-number gas flow through pipelines with side branch cavities. *AIAA Paper* 86-1924.

BURSTYN, W. 1922 Eine neue Pfeife (a new pipe). *Z. Tech. Phys.* **3**, 179–180.

CADWELL, L. H. 1994 Singing corrugated pipes revisited. *Am. J. Phys.* **62**, 224–227.

CERMAK, P. 1922 Über die Tonbildung bei Metallschläuchen mit eingedräcktem Spiralgang (On the sound generation in flexible metal hoses with spiraling grooves). *Phys. Z.* **23**, 394–397.

CRAWFORD, F. S. 1974 Singing corrugated pipes. *Am. J. Phys.* **62**, 278–288.

CURLE, N. 1955 The influence of solid boundaries upon aerodynamic sound. *Proc. R. Soc. Lond.* A **231**, 505–514.

DEQUAND, S., HULSHOFF, S. J. & HIRSCHBERG, A. 2003a Self-sustained oscillations in a closed side branch system. *J. Sound Vib.* **265**, 359–386.

DEQUAND, S., LUO, X., WILLEMS, J. F. H. & HIRSCHBERG, A. 2003b Helmholtz-like resonator self-sustained oscillations. Part 1. *AIAA J.* **41** (3), 408–415.

DERKS, M. M. G. & HIRSCHBERG, A. 2004 Self-sustained oscillation of the flow along Helmholtz resonators in a tandem configuration. In *Proc. 8th Intl Conf. on Flow-Induced Vibration (FIV2004), Paris, 6–9 July* (ed. E. de Langre & F. Axisa), pp. 435–440. Polytechnique.

EGGELS, J. G. M., UNGER, F., WEISS, M. H., WESTERWELL, J., ADRIAN, R. J., FRIEDRICH, R. & NIEUWSTADT, F. T. M. 1994 Fully developed turbulent pipe flow: a comparison between direct numerical simulation and experiment. *J. Fluid Mech.* **268**, 175–209.

ELDER, S. A., FARABEE, T. M. & DEMETZ, F. C. 1982 Mechanisms of flow-excited cavity tones at low Mach number. *J. Acoust. Soc. Am.* **72** (2), 532–549.

ELLIOTT, J. W. 2005 Corrugated pipe flow. In *Lecture Notes on the Mathematics of Acoustics* (ed. M. C. M. Wright), pp. 207–222. Imperial College Press.

FLETCHER, J. C. 1979 Air flow and sound generation in musical wind instruments. *Annu. Rev. Fluid Mech.* **11**, 95–121.

GLOERFELT, X. 2009 *Cavity Noise.* von Karman Lecture Notes on Aerodynamic Noise from Wall-Bounded Flows. Von Karman Institute.

GOLLIARD, J. 2002 Noise of Helmholtz-resonator like cavities excited by low Mach-number turbulent flows. PhD thesis, École Supérieure d'Ingénieurs de Poitiers, Poitiers, France.

GOLLIARD, J., TONON, D. & BELFROID, S. P. C. 2010 Experimental investigation of the source locations for whistling short corrugated pipes. In *Proc. ASME 2010 3rd Joint US–European*

Fluids Engineering Summer Meeting and 8th Intl Conf. on Nanochannels, Microchannels and Minichannels, Montreal, Canada.

GOYDER, H. 2009 *On the Modelling of Noise Generation in Corrugated Pipes*. ASME Pressure Vessels and Piping Division, Prague, Czech Republic.

GUTIN, L. 1948 On the sound field of a rotating propeller. (Original in Russian: *Z. Tekh. Fiz.* 1936; **12**, 76–83.) *NACA Tech. Memo.* 1195.

HOFMANS, G. C. 1998 Vortex sound in confined flows. PhD thesis, Eindhoven University of Technology, Eindhoven, the Netherlands.

HOWE, M. S. 1980 The dissipation of sound at an edge. *J. Sound Vib.* **70**, 407–411.

HOWE, M. S. 1998 *Acoustics of Fluid–Structure Interactions*. Cambridge University Press.

INGARD, U. & SINGHAL, V. K. 1975 Effect of flow on the acoustic resonances of an open-ended duct. *J. Acoust. Soc. Am.* **58** (4), 788–793.

KELLER, J. J. 1984 Non-linear self-excited acoustic oscillations in cavities. *J. Sound Vib.* **94**, 397–409.

KOOIJMAN, G., HIRSCHBERG, A. & GOLLIARD, J. 2008 Acoustical response of orifices under grazing flow: effect of boundary layer profile and edge geometry. *J. Sound Vib.* **315**, 849–874.

KOP'EV, V. F., MIRONOV, M. A. & SOLNTSEVA, V. S. 2008 Aeroacoustic interaction in a corrugated duct. *Acoust. Phys.* **54**, 197–203.

KRIESELS, P. C., PETERS, M. C. A. M., HIRSCHBERG, A., WIJNANDS, A. P. J., IAFRATI, A., RICCARDI, G., PIVA, R. & BRUGGEMAN, J. C. 1995 High amplitude vortex-induced pulsations in a gas transport system. *J. Sound Vib.* **184**, 343–368.

KRISTIANSEN, U. R. & WIIK, G. A. 2007 Experiments on sound generation in corrugated pipes with flow. *J. Acoust. Soc. Am.* **121**, 1337–1344.

MARTÍNEZ-LERA, P., SCHRAM, C., FÖLLER, S., KAESS, R. & POLIFKE, W. 2009 Identification of the aeroacoustic response of a low Mach number flow through a T-joint. *J. Acoust. Soc. Am.* **126** (2), 582–586.

MICHALKE, A. 1965 On spatially growing disturbances in an inviscid shear layer. *J. Fluid Mech.* **23** (3), 521–544.

MUNT, R. M. 1977 The interaction of sound with a subsonic jet issuing from a semi-infinite cylindrical pipe. *J. Fluid Mech.* **83**, 609–640.

MUNT, R. M. 1990 Acoustic transmission properties of a jet pipe with subsonic jet flow. Part I. The cold jet reflection coefficient. *J. Sound Vib.* **142**, 413–436.

MYERS, M. K. 1986 An exact energy corollary for homentropic flow. *J. Sound Vib.* **109** (2), 277–284.

MYERS, M. K. 1991 Transport of energy by disturbances in arbitrary steady flows. *J. Fluid Mech.* **226**, 383–400.

NAKAMURA, Y. & FUKAMACHI, N. 1991 Sound generation in corrugated tubes. *Fluid Dyn. Res.* **7**, 255–261.

NAKIBOĞLU, G., BELFROID, S. P. C., TONON, D., WILLEMS, J. F. H. & HIRSCHBERG, A. 2009 *A Parametric Study on the Whistling of Multiple Side Branch System as a Model for Corrugated Pipes*. ASME Pressure Vessels and Piping Division.

NAKIBOĞLU, G., BELFROID, S. P. C., WILLEMS, J. F. H. & HIRSCHBERG, A. 2010 Whistling behavior of periodic systems: corrugated pipes and multiple side branch system. *Intl J. Mech. Sci.* **52** (11), 1458–1470.

OSHKAI, P., ROCKWELL, D. & POLLACK, M. 2005 Shallow cavity flow tones: transformation from large- to small-scale modes. *J. Sound Vib.* **280**, 777–813.

PATANKAR, S. V. & SPALDING, D. B. 1972 A calculation procedure for heat mass and momentum transfer in three-dimensional parabolic flows. *Intl J. Heat Mass Transfer* **15**, 1787–1806.

PETERS, M. C. A. M., HIRSCHBERG, A., REIJNEN, A. J. & WIJNANDS, A. P. J. 1993 Damping and reflection coefficient measurements for an open pipe at low Mach and low Helmholtz numbers. *J. Fluid Mech.* **256**, 499–534.

PETRIE, A. M. & HUNTLEY, I. D. 1980 The acoustic output produced by a steady airflow through a corrugated duct. *J. Sound Vib.* **70** (1), 1–9.

PIERCE, A. D. 1981 *Acoustics*. McGraw Hill.

POPESCU, M. & JOHANSEN, S. T. 2008 Acoustic wave propagation in low Mach flow pipe. *AIAA Paper* 2008-0063.

RAYLEIGH, LORD 1945 *Lecture Notes on the Mathematics of Acoustics*. Dover.

ROCKWELL, D. 1983 Oscillations of impinging shear layers. *AIAA J.* **21**, 645–664.

ROCKWELL, D., LIN, C. J., OSHKAI, P., REISS, M. & POLLACK, M. 2003 Shallow cavity flow tone experiments: onset of locked-on states. *J. Fluids Struct.* **17**, 381–414.

ROWLEY, C. W., WILLIAMS, D. R., COLONIUS, T., MURRAY, R. M. & MACMYNOWSKI, D. G. 2006 Linear models for control of cavity flow oscillations. *J. Fluid Mech.* **547**, 317–330.

SAROHIA, V. 1977 Experimental investigation of oscillations in flow over shallow cavities. *AIAA J.* **15** (7), 984–991.

SCHLICHTING, H. 1979 *Boundary Layer Theory*. McGraw Hill.

SERAFIN, S. & KOJS, J. 2005 Computer models and compositional applications of plastic corrugated tubes. *Organised Sound* **10** (1), 67–73.

SILVERMAN, M. P. & CUSHMAN, G. M. 1989 Voice of the dragon: the rotating corrugated resonator. *Eur. J. Phys.* **10**, 298–304.

TAM, C. K. W. & BLOCK, P. J. W. 1978 On the tones and pressure oscillations induced by flow over rectangular cavities. *J. Fluid Mech.* **89**, 373–399.

TONON, D., LANDRY, B. J. T., BELFROID, S. P. C., WILLEMS, J. F. H, HOFMANS, G. C. J. & HIRSCHBERG, A. 2010 Whistling of a pipe system with multiple side branches: comparison with corrugated pipes. *J. Sound Vib.* **329**, 1007–1024.

ZIADA, S. & BÜHLMANN, E. T. 1991 Flow-induced vibration in long corrugated pipes. In *Intl Conf. on Flow-Induced Vibrations*. IMechE, UK.

ZIADA, S., NG, H. & BLAKE, C. E. 2003 Flow excited resonance of a confined shallow cavity in low Mach number flow and its control. *J. Fluids Struct.* **18**, 79–92.

ZIADA, S. & SHINE, S. 1999 Strouhal numbers of flow-excited acoustic resonance of closed side branches. *J. Fluids Struct.* **13**, 127–142.